Models for the two-phase flow of concentrated suspensions†

T O B I A S   A H N E R T [1], A N D R E A S   M Ü N C H [2] and B A R B A R A   W A G N E R [1]

[1]*Institute of Mathematics, Technische Universität Berlin, Strasse des 17. Juni 136, Berlin 10623, Germany*
emails: ahnert@math.tu-berlin.de, muench@maths.ox.ac.uk, bwagner@math.tu-berlin.de
[2]*Mathematical Institute, 24–29 St Giles, Oxford OX1 3LB, UK*
email: muench@maths.ox.ac.uk

A new two-phase model for concentrated suspensions is derived that incorporates a constitutive law combining the rheology for non-Brownian suspension and granular flow. The resulting model exhibits a yield-stress behaviour for the solid phase depending on the collision pressure. This property is investigated for the simple geometry of plane Poiseuille flow, where an unyielded or jammed zone of finite width arises in the centre of the channel. For the steady states of this problem, the governing equations are reduced to a boundary value problem for a system of ordinary differential equations and the conditions for existence of solutions with jammed regions are investigated using phase-space methods. For the general time-dependent case a new drift-flux model is derived using matched asymptotic expansions that takes into account the boundary layers at the walls and the interface between the yielded and unyielded region. The drift-flux model is used to numerically study the dynamic behaviour of the suspension flow, including the appearance and evolution of an unyielded or jammed regions.

Key words: Suspensions, jamming, yield stress, averaging, multiphase model, phase-space methods, matched asymptotics, drift-flux.

1 Introduction

Ever since the derivation of an effective viscosity for dilute suspensions by Einstein [18] and its extensions by Batchelor & Green [4], there have been numerous investigations into the rheological properties of suspensions. Since the experimental work by Gadala-Maria & Acrivos [20] and Leighton & Acrivos [31], the discovery of physical phenomena related to shear-induced particle migration for concentrated suspensions from regions of high to low stress has spurred theoretical investigations that led to expressions for associated diffusive flux terms as well as drift-flux models, see, for example, [10, 31, 35, 39].

Even though drift-flux models are quite popular and are frequently used as a transport mechanism [11, 36, 54], they sometimes predict unphysical migration behaviour such as a sharp peak in the particle volume fraction profile in the centre of flow through a channel,

where the shear rate vanishes [37], whereas in experiments [22] the concentration profile is in fact flattened there. While these issues were addressed by introducing a suspension temperature as a measure of particle velocity fluctuations [28, 37, 52], or by slightly changing parameter values such as the exponent in the Krieger–Dougherty law or in the expressions for the relative suspension viscosity and the particulate phase pressure as the maximum packing fraction is approached [45], it remains to understand how these models can be based on their underlying two-phase models. This has been particularly difficult for highly concentrated suspensions, when additional flow transitions, such as jammed states may occur. Some fundamental studies of these flow regimes have been presented in Cassar *et al.* [9], where it was shown that for highly dense suspensions of particles in a viscous liquid that is sheared at a rate $\dot{\gamma}$ under a confining pressure p_p can be characterized by a single dimensionless control parameter, the 'viscous number' $I_v = \eta_f \dot{\gamma}/p_p$, where η_f is the fluid viscosity. These findings have been supported by experiments where the suspensions are sheared with a constant particle pressure [5]. Their results show that, indeed, the friction and volume-fraction law collapse onto universal curves when expressed in terms of the dimensionless number I_v. By including hydrodynamic contributions, Boyer *et al.* propose a model for the whole range of I_v, which has been discussed by [12], and also by Trulsson *et al.* [48]. An earlier review of stress terms for dense suspensions can be found in [47] and more recently for the special case of Houska fluids analytical solutions for unidirectional pipe flow have been derived in [1], while other approaches such as by Quemada in [41–44] introduce structural models for concentrated suspensions, where shear-dependent effective volume fractions are introduced to take account of structures of the flow, such as clusters into account.

Boyer *et al.* formulate their model in a form, where the shear stress and particle pressure are expressed in terms of the strain rate and the volume fraction. Their expressions for the shear and normal viscosities are similar to the ones found in Morris & Boulay [35], and also Miller *et al.* [34], who investigated more general curvilinear flows, where the migration behaviour was accommodated by allowing for anisotropy in the normal stresses.

In Section 2, we derive a new two-phase model for non-homogeneous shear flows that captures the flow properties of non-Brownian dense suspensions by including the constitutive equations proposed by Boyer *et al.* [5]. The derivation is based on the averaging framework as given in Drew & Passman [14, 16] and is formulated for a general three-dimensional flow. For the remainder of the article, we focus on the pressure-driven plane Poiseuille flow as our model example for non-constant shear flows and investigate the flow behaviour predicted by the two-phase model as the particle volume fraction is varied.

In Section 3, we first consider stationary solutions for the plane Poiseuille flow, for which the model reduces to a boundary-value problem for a system of ordinary differential equations. Using phase-space methods, we reveal the existence of solutions that show an unyielded region similar due to a yield-stress condition for the solid phase that is similar to the condition in Bingham-type flows. In this region, located at the centre of the channel, the solid volume fraction is at its maximum and the solid phase has jammed to form a porous matrix through which the fluid phase can still flow through. We study the dependence of the width of the unyielded i.e., jammed region (for the solid phase) and the flow fields for both phases upon varying the flow parameters. We then show that for

typical ranges of the parameter $\mathrm{Da} = L/K_p \ll O(1)$ the flow field develops boundary layers at the channel walls and at the interface between the unyielded and yielded regions, where L is the characteristic scale of the channel width and K_p is proportional to the particle size. Using matched asymptotic analysis as $\mathrm{Da} \to \infty$, we obtain an expression for the flow field.

In Section 4, we generalize this analysis and for the first time present a systematic asymptotic derivation of a time-dependent drift-flux model via matched asymptotic expansions. Our numerical simulations of the drift-flux model captures the emergence of a jammed region and the evolution of the flow and phase field into a stationary state.

In Section 5, we summarize our results and give an outlook on future directions for research.

2 Formulation of the two-phase model

We consider two inert phases, a solid phase of particles suspended in a liquid phase where we denote with $k \in \{s, f\}$, the solid phase by s and the liquid phase by f. Inside each phase the balance equations for mass and momentum

$$\partial_t \rho_k + \nabla \cdot (\rho_k \boldsymbol{u}_k) = 0, \tag{2.1a}$$

$$\partial_t (\rho_k \boldsymbol{u}_k) + \nabla \cdot (\rho_k \boldsymbol{u}_k \otimes \boldsymbol{u}_k) - \nabla \cdot \boldsymbol{T}_k - \boldsymbol{f}_k = \boldsymbol{0}, \tag{2.1b}$$

are satisfied together with the two jump conditions (see, e.g., [26])

$$\sum_k \rho_k (\boldsymbol{u}_k - \boldsymbol{u}_i) \cdot \boldsymbol{n}_k = 0, \tag{2.1c}$$

$$\sum_k \rho_k \boldsymbol{u}_k (\boldsymbol{u}_k - \boldsymbol{u}_i) \cdot \boldsymbol{n}_k - \boldsymbol{T}_k \cdot \boldsymbol{n}_k = \boldsymbol{0}, \tag{2.1d}$$

at the interfaces of the phases with $\boldsymbol{n}_k$ denoting the unit normal pointing out of phase k and $\boldsymbol{u}_i$ is the interface velocity. The quantities ρ, $\boldsymbol{u}$, $\mathbf{T}$ and $\mathbf{f}$ denote density, velocity, stress tensor and body force density in each phase, respectively. At an interface $\boldsymbol{u}_k$ is defined as

$$\boldsymbol{u}_k(\boldsymbol{x}^*, t) \equiv \lim_{\boldsymbol{x} \to \boldsymbol{x}^*; \boldsymbol{x} \in K} \boldsymbol{u}(x, t),$$

where K denotes the set of points occupied by phase k, and similarly for the other quantities.

In deriving a two-phase model, essentially three different averaging approaches have been pursued in the literature. The volume average, the time average and the ensemble average (sometimes also called statistical average). Although all three produce similar balance equation for the phases their derivation and closure is distinct. Besides the ensemble averaging developed by Drew & Passman in [16] and [14], volume averaging is treated in Kolev [30] and Whitaker [50] and time averaging in Ishii *et al.* [26].

For the derivation of our two-phase model, we follow the mathematical framework by

Drew [14] and Drew and Passman [16] and introduce a component indicator function

$$X_k(\boldsymbol{x},t) = \begin{cases} 1, & \text{if } (\boldsymbol{x},t) \in K \\ 0, & \text{if } (\boldsymbol{x},t) \notin K, \end{cases} \qquad (2.2)$$

with K the set of states of the kth-phase to define the averaged quantities

$$\phi_k \equiv \langle X_k \rangle, \quad \overline{\rho}_k \equiv \frac{\langle X_k \rho \rangle}{\phi_k}, \quad \widehat{\boldsymbol{u}}_k \equiv \frac{\langle X_k \rho \boldsymbol{u} \rangle}{\phi_k \overline{\rho}_k}, \quad \overline{p}_k \equiv \frac{\langle X_k p \rangle}{\phi_k}, \quad \overline{\boldsymbol{\tau}}_k \equiv -\frac{\langle X_k \boldsymbol{\tau} \rangle}{\phi_k}, \qquad (2.3)$$

which denote the volume fractions, the averaged densities, velocities, pressures and deviatoric stresses, respectively. For these quantities, we then derive the following balance equations

$$\partial_t \phi_s + \nabla \cdot (\phi_s \widehat{\boldsymbol{u}}_s) = 0, \qquad (2.4a)$$

$$\partial_t \phi_f + \nabla \cdot (\phi_f \widehat{\boldsymbol{u}}_f) = 0, \qquad (2.4b)$$

$$\overline{\rho}_s \partial_t (\phi_s \widehat{\boldsymbol{u}}_s) + \nabla \cdot (\phi_s \overline{\rho}_s \widehat{\boldsymbol{u}}_s \otimes \widehat{\boldsymbol{u}}_s) \qquad (2.4c)$$

$$-\nabla \cdot (\phi_s \overline{\boldsymbol{\tau}}_s) + \nabla (\phi_s \overline{p}_s) = M_s^d + \overline{p}_f \nabla \phi_s, \qquad (2.4d)$$

$$\overline{\rho}_f \partial_t (\phi_f \widehat{\boldsymbol{u}}_f) + \nabla \cdot (\phi_f \overline{\rho}_f \widehat{\boldsymbol{u}}_f \otimes \widehat{\boldsymbol{u}}_f) \qquad (2.4e)$$

$$-\nabla \cdot (\phi_f \overline{\boldsymbol{\tau}}_f) + \nabla (\phi_f \overline{p}_f) = -M_s^d + \overline{p}_f \nabla \phi_f. \qquad (2.4f)$$

The detailed derivation is given in Appendix A, where we note that in the present study we also have neglected the Reynolds stresses (see Drew [15]) and their possible impact on dispersion and boundary layers.

2.1 Constitutive equations for a dense suspension

To close the model for the flow in the bulk, we need to specify constitutive equations besides the assumptions already made. Essentially, we need four relations for the pressure difference and stress between the phases $\overline{p}_s - \overline{p}_f$ and M_s^d, and for the stresses in each phase, $\overline{\boldsymbol{\tau}}_f$ and $\overline{\boldsymbol{\tau}}_s$. In addition, to simplify notation, we set $\phi \equiv \phi_s$.

For the momentum transfer

$$M_s^d = \frac{\mu_f \phi^2}{K_p (1-\phi)} (\widehat{\boldsymbol{u}}_f - \widehat{\boldsymbol{u}}_s), \qquad (2.5)$$

we have used the Kozeny–Carman equation, with K_p depending on the particle diameter, $K_p \propto a^2$, see, e.g., [6]. We note that more general closures could have been used for a wider range of ϕ_s, in particular for the medium range, see, for example, [21] and references therein and also [2].

The constitutive law for the remaining quantities extend the model for dense suspensions given by Boyer *et al.* [5] for shear flow to a general flow situation. We state it in terms of the (weighted) solid contact pressure, defined here as

$$p_c \equiv \phi (\overline{p}_s - \overline{p}_f), \qquad (2.6)$$

and the shear rate tensors for each phase

$$\dot{\boldsymbol{\gamma}}_f \equiv [\nabla \widehat{\boldsymbol{u}}_f + (\nabla \widehat{\boldsymbol{u}}_f)^T], \qquad \dot{\boldsymbol{\gamma}}_s \equiv [\nabla \widehat{\boldsymbol{u}}_s + (\nabla \widehat{\boldsymbol{u}}_s)^T]. \tag{2.7}$$

For the liquid phase stress, we have

$$\overline{\boldsymbol{\tau}}_f = \mu_f \dot{\boldsymbol{\gamma}}_f + (\mu^* - \frac{2}{3}\mu_f)(\nabla \cdot \widehat{\boldsymbol{u}}_f)\boldsymbol{I}, \tag{2.8a}$$

where μ_f denotes the viscosity of the pure liquid. The second term in the relation for $\overline{\boldsymbol{\tau}}_f$ will be dropped by setting the bulk viscosity $\mu^* = \frac{2}{3}\mu_f$. This particular choice has no influence on the solutions, since generally the bulk viscosity vanishes for stationary flows and does not appear in the leading order approximation of the derived drift-flux term.

For the solid phase, we need to consider two cases for the constitutive law: Either $|\dot{\boldsymbol{\gamma}}_s| > 0$, then

$$\overline{\boldsymbol{\tau}}_s = \mu_f \eta_s(\phi) \dot{\boldsymbol{\gamma}}_s, \tag{2.8b}$$

$$p_c = \mu_f \eta_n(\phi) |\dot{\boldsymbol{\gamma}}_s|, \tag{2.8c}$$

with

$$\eta_s(\phi) = 1 + \frac{5}{2} \frac{\phi_{sc}}{\phi_{sc} - \phi} + \mu_c(\phi) \frac{\phi}{(\phi_{sc} - \phi)^2}, \tag{2.8d}$$

$$\mu_c(\phi) = \mu_1 + \frac{\mu_2 - \mu_1}{1 + I_0 \phi^2 (\phi_{sc} - \phi)^{-2}}, \tag{2.8e}$$

$$\eta_n(\phi) = \left(\frac{\phi}{\phi_{sc} - \phi} \right)^2, \tag{2.8f}$$

where for tensors $\boldsymbol{a}$, we define the norm as $|\boldsymbol{a}| = (\frac{1}{2} \sum_{j,k} |a_{jk}|^2)^{1/2}$. The parameters $\mu_2 \geqslant \mu_1 > 0$, $I_0 \geqslant 0$ characterize the contact contribution in the expression for η_s, and ϕ_{sc} is the maximum volume fraction for the solid phase, which is attained when the solid phase jams. We note from the experimentally fitted laws in Boyer *et al.* [5], (2.8d)–(2.8f) is found from the friction law for dense suspensions $\mu_s = \mu_1 + (\mu_2 - \mu_1)/(1 + I_0/I_v) + I_v + 5/2\phi_{sc}I_v^{1/2}$ scaled by $I_v = [(\phi_{sc} - \phi)/\phi]^2$.

For the other case $\dot{\boldsymbol{\gamma}}_s = 0$, we require

$$\phi = \phi_{sc}, \tag{2.8g}$$

while $\overline{\boldsymbol{\tau}}_s$, $\overline{p}_s$ and $\overline{p}_f$ are left unspecified, except for the constraint

$$|\phi \overline{\boldsymbol{\tau}}_s| \leqslant \mu_1 p_c. \tag{2.8h}$$

Conversely, if (2.8h) is satisfied, then it follows from equations (2.8b) to (2.8f) that $|\dot{\boldsymbol{\gamma}}_s|$ cannot be positive. Thus, if the collision pressure p_c is finite, our model for concentrated suspensions is capable of exhibiting regions where the solid phase is jammed, whenever $|\overline{\boldsymbol{\tau}}_s|$ drops below a certain yield stress. In the jammed region, the solid phase flow is plug-like. This is similar to the plug-like flow in a Bingham model, which, however, describes single-phase rheology with a constant yield stress.

The jammed regions are separated from the regions where $|\dot{\boldsymbol{\gamma}}_s| > 0$ by yield surfaces. Across a yield surface, we require ϕ, $\widehat{\boldsymbol{u}}_f$, $\widehat{\boldsymbol{u}}_s$, $(-\overline{p}_f \boldsymbol{I} + \overline{\boldsymbol{\tau}}_f) \cdot \boldsymbol{n}_y$, $(-\overline{p}_s \boldsymbol{I} + \overline{\boldsymbol{\tau}}_s) \cdot \boldsymbol{n}_y$ and $|\dot{\boldsymbol{\gamma}}_s|$ to be continuous, where $\boldsymbol{n}_y$ denotes the unit normal vector to the surface.

2.2 Non-dimensionalization

We introduce characteristic scales via

$$x = Lx', \qquad y = Ly', \qquad z = Lz', \qquad t = \frac{L}{U}t', \tag{2.9}$$

$$\boldsymbol{u}_k = U\boldsymbol{u}'_k, \qquad p_k = \frac{U\mu_f}{L}p'_k, \qquad \boldsymbol{\tau}_k = \frac{U\mu_f}{L}\boldsymbol{\tau}'_k, \tag{2.10}$$

for $k = s, f$. After non-dimensionalization, we drop the primes and also the bars and hats indicating averaging, and obtain the system

$$\partial_t(1 - \phi) + \nabla \cdot ((1 - \phi)\boldsymbol{u}_f) = 0, \tag{2.11a}$$

$$\partial_t \phi + \nabla \cdot (\phi \boldsymbol{u}_s) = 0, \tag{2.11b}$$

$$\mathrm{Re}[\partial_t((1 - \phi)\boldsymbol{u}_f) + \nabla \cdot ((1 - \phi)\boldsymbol{u}_f \otimes \boldsymbol{u}_f)] \tag{2.11c}$$

$$- \nabla \cdot (\phi_f \boldsymbol{\tau}_f) + (1 - \phi)\nabla p_f = -\mathrm{Da}\, \frac{\phi^2}{(1 - \phi)}(\boldsymbol{u}_f - \boldsymbol{u}_s),$$

$$\frac{\mathrm{Re}}{r}[\partial_t(\phi \boldsymbol{u}_s) + \nabla \cdot (\phi \boldsymbol{u}_s \otimes \boldsymbol{u}_s)] \tag{2.11d}$$

$$- \nabla \cdot (\phi \boldsymbol{\tau}_s) + \phi \nabla p_f + \nabla p_c = \mathrm{Da}\, \frac{\phi^2}{(1 - \phi)}(\boldsymbol{u}_f - \boldsymbol{u}_s).$$

Three dimensionless numbers appear here, namely the Reynolds number $\mathrm{Re} = UL\rho_f/\mu_f$, the Darcy number $\mathrm{Da} = L^2/K_p$ and the density ratio $r = \rho_f/\rho_s$. We focus on the case where liquid and solid phases are density matched and set $r = 1$.

The non-dimensional versions of the constitutive equations for the rheology are now as follows: For the liquid phase, we have

$$\boldsymbol{\tau}_f = \dot{\boldsymbol{\gamma}}_f. \tag{2.12a}$$

For the solid phase, either $|\dot{\boldsymbol{\gamma}}_s| > 0$, then

$$\boldsymbol{\tau}_s = \eta_s(\phi)\dot{\boldsymbol{\gamma}}_s, \tag{2.12b}$$

$$p_c = \eta_n(\phi)|\dot{\boldsymbol{\gamma}}_s|, \tag{2.12c}$$

with (2.8d)–(2.8f); or $\dot{\boldsymbol{\gamma}}_s = 0$, and then we require

$$\phi = \phi_{\mathrm{sc}}$$

and

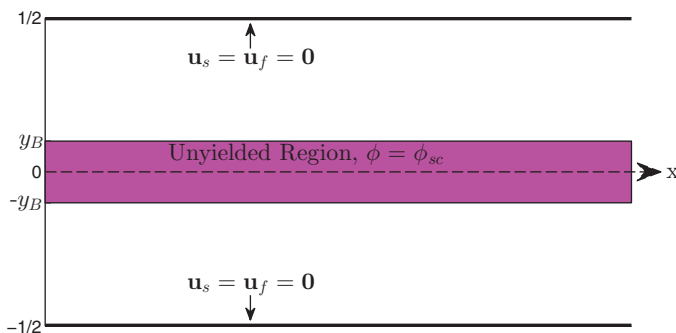$$|\phi \boldsymbol{\tau}_s| \leqslant \mu_1 p_c.$$

FIGURE 1. Sketch of the flow situation in a channel.

The continuity conditions across yield surfaces carry over from the dimensional equations and also the parameters, μ_1, μ_2 and I_0 and ϕ_{sc}, which were non-dimensional to begin with.

3 Plane Poiseuille flow

It is instructive to investigate the properties of the model (2.11) for one of the classical flow situations, namely, plane Poiseuille or channel flow, which we think is the simplest flow geometry to exhibit the emergence of a jammed or unyielded regions. The dimensions of the channel are $0 < x < x_e$ and $-\frac{1}{2} < y < \frac{1}{2}$, where we have used the channel with for the length scale L, and prescribe for the inlet conditions at $x = 0$

$$\phi = \phi_{in}, \quad \boldsymbol{u}_f = \begin{pmatrix} u_{f,in}\left(\frac{1}{4} - y^2\right) \\ 0 \end{pmatrix}, \quad \boldsymbol{u}_s = \begin{pmatrix} u_{s,in}\left(\frac{1}{4} - y^2\right) \\ 0 \end{pmatrix}, \tag{3.1}$$

and for the outlet condition at $x = x_e$,

$$\mathbf{n} \cdot (p_s \boldsymbol{I} + \phi \eta_s (\nabla \boldsymbol{u}_s)^T) = 0, \quad \mathbf{n} \cdot (p_f \boldsymbol{I} + (1 - \phi)\eta_s (\nabla \boldsymbol{u}_s)^T) = 0. \tag{3.2}$$

Moreover, we can set $u_{f,in} = 1$ by appropriately choosing the velocity scale U. In addition, we only consider rectilinear flow, so the inertial terms vanish and we obtain for the bulk equations

$$\partial_t (1 - \phi) + \nabla \cdot ((1 - \phi)\boldsymbol{u}_f) = 0, \tag{3.3a}$$

$$\partial_t \phi + \nabla \cdot (\phi \boldsymbol{u}_s) = 0, \tag{3.3b}$$

$$-\nabla \cdot ((1 - \phi)\boldsymbol{\tau}_f) + (1 - \phi)\nabla p_f = -\mathrm{Da}\frac{\phi^2}{(1 - \phi)}(\boldsymbol{u}_f - \boldsymbol{u}_s), \tag{3.3c}$$

$$-\nabla \cdot (\phi \boldsymbol{\tau}_s) + \phi \nabla p_f + \nabla p_c = \mathrm{Da}\frac{\phi^2}{(1 - \phi)}(\boldsymbol{u}_f - \boldsymbol{u}_s), \tag{3.3d}$$

where

$$\boldsymbol{\tau}_f = \dot{\boldsymbol{\gamma}}_f \tag{3.4a}$$

$$|\phi\boldsymbol{\tau}_s| \leqslant \mu_1 p_c, \qquad \phi = \phi_{sc} \qquad \text{if } |\dot{\boldsymbol{\gamma}}_s| = 0 \tag{3.4b}$$

$$\boldsymbol{\tau}_s = \eta_s(\phi)\dot{\boldsymbol{\gamma}}_s, \qquad p_c = \eta_n(\phi)|\dot{\boldsymbol{\gamma}}_s| \qquad \text{if } |\dot{\boldsymbol{\gamma}}_s| \neq 0. \tag{3.4c}$$

At the channel walls, we assume the no-slip conditions

$$\boldsymbol{u}_s = \boldsymbol{0}, \qquad \boldsymbol{u}_f = \boldsymbol{0}. \tag{3.5}$$

For the two-phase model at hand, it turns out to be advantageous to formulate the problem in terms of the flow variables

$$\boldsymbol{v} \equiv (1 - \phi)\boldsymbol{u}_f + \phi\boldsymbol{u}_s, \qquad \boldsymbol{w} \equiv \boldsymbol{u}_f - \boldsymbol{u}_s. \tag{3.6}$$

In these variables, noting that $\boldsymbol{v} + \phi\boldsymbol{w} = \boldsymbol{u}_f$, $\boldsymbol{v} - (1 - \phi)\boldsymbol{w} = \boldsymbol{u}_s$ the problem can be written as

$$\nabla \cdot \boldsymbol{v} = 0, \tag{3.7a}$$

$$\partial_t \phi + \nabla \cdot (\phi\boldsymbol{v} - \phi(1 - \phi)\boldsymbol{w}) = 0, \tag{3.7b}$$

$$-\nabla \cdot \left((1 - \phi)\dot{\boldsymbol{\gamma}}_f\right) + (1 - \phi)\nabla p_f = -\mathrm{Da}\frac{\phi^2}{1 - \phi}\boldsymbol{w}, \tag{3.7c}$$

$$-\nabla \cdot (\phi\boldsymbol{\tau}_s) + \phi\nabla p_f + \nabla p_c = \mathrm{Da}\frac{\phi^2}{(1 - \phi)}\boldsymbol{w}, \tag{3.7d}$$

where $\boldsymbol{\tau}_s$ satisfies the constitutive law (3.4b), (3.4c). At the walls $y = \pm\frac{1}{2}$, the no-slip conditions are

$$\boldsymbol{v} = \boldsymbol{0}, \qquad \boldsymbol{w} = \boldsymbol{0}. \tag{3.7e}$$

3.1 Formulation of the stationary problem

For the system (3.7a)–(3.7e), we now derive conditions for the existence of stationary two-dimensional solutions where all quantities, except for the pressure, depend only on y,

$$\phi = \phi(y), \qquad \boldsymbol{v} = \boldsymbol{v}(y), \qquad \boldsymbol{w} = \boldsymbol{w}(y), \tag{3.8}$$

$$\boldsymbol{\tau}_f = \boldsymbol{\tau}_f(y), \qquad \boldsymbol{\tau}_s = \boldsymbol{\tau}_s(y), \qquad p_f = p_f(x, y). \tag{3.9}$$

The combination of no-slip boundary conditions (3.7e) with (3.7a), (3.7b) yields (if v_1, v_2 and w_1, w_2 denote the components of the vectors $\boldsymbol{v}$ and $\boldsymbol{w}$, respectively.)

$$v_2 = 0, \qquad\qquad w_2 = 0, \tag{3.10}$$

therefore

$$\dot{\gamma}_s = \begin{pmatrix} 0 & \partial_y(v_1 - (1-\phi)w_1) \\ \partial_y(v_1 - (1-\phi)w_1) & 0 \end{pmatrix}, \tag{3.11a}$$

$$\dot{\gamma}_f = \begin{pmatrix} 0 & \partial_y(v_1 + \phi w_1) \\ \partial_y(v_1 + \phi w_1) & 0 \end{pmatrix}. \tag{3.11b}$$

The momentum balances (3.7c) and (3.7d) become, in components,

$$-\partial_y\big((1-\phi)\partial_y(v_1 + \phi w_1)\big) + (1-\phi)\partial_x p_f = -\mathrm{Da}\frac{\phi^2}{(1-\phi)}w_1, \tag{3.12a}$$

$$\partial_y p_f = 0, \tag{3.12b}$$

$$-\partial_y\left(\phi\tau_{s12}\right) + \phi\partial_x p_f + \partial_x p_c = \mathrm{Da}\frac{\phi^2}{(1-\phi)}w_1, \tag{3.12c}$$

$$-\partial_y\left(\phi\tau_{s22}\right) + \phi\partial_y p_f + \partial_y p_c = 0. \tag{3.12d}$$

From (3.12b), we conclude that $p_f = p_f(x)$ is a function of x only, and the same is true for $\phi\tau_{s22} + \partial_y p_c = c_1(x)$. The momentum balance requires continuity of stresses and hence these two relations must be satisfied even across yield surfaces. If we assume that the solid is not stagnant everywhere, that is, (3.4c) holds for some y, we can deduce (because of (3.11a)) that $\tau_{s22} = 0$ there and hence $p_c = c_1(x)$ and $\tau_{s22} = 0$ everywhere. Using now the second condition in (3.4c) we see that, because the right hand side depends only on y, p_c must in fact be a constant, which is free and thus acts as an additional parameter. Using this in (3.7c), (3.7d) and adding the two equations gives

$$\partial_x p_f = \partial_y \tau_{12}, \tag{3.13}$$

where we have introduced the total stress $\tau \equiv (1-\phi)\tau_f + \phi\tau_s = (1-\phi)\dot{\gamma}_f + \phi\tau_s$. Since the left-hand side only depends on x and the right-hand side only on y, both have to be constant, and we get

$$p_f(x) = p_1 x + p_0, \tag{3.14a}$$

where p_0 is a constant of integration, which by a choice of origin, we can assume, without loss of generality, to be zero, and

$$\tau_{12}(y) = p_1 y. \tag{3.14b}$$

Here and from now on, we will only look at the case of solutions with velocities and volume fractions that are symmetric with respect to $y = 0$, so that we have in particular set the integration constant that would normally appear in (3.14b) to 0 and will only consider one half of the channel, $0 \leqslant y \leqslant 1/2$. Moreover, we assume that we have at most one unyielded region $0 \leqslant y \leqslant y_B$ that is located at the centre of the channel and ends at y_B, $0 \leqslant y_B \leqslant 1/2$, which is an unknown of the problem.

Overall we get the system: For $y \in [y_B; 1/2]$, ϕ, τ_{s12}, τ_{f12}, v_1 and w_1 satisfy

$$\partial_y((1 - \phi)\tau_{f12}) = (1 - \phi)p_1 + \mathrm{Da}\,\frac{\phi^2}{1 - \phi}w_1, \tag{3.15a}$$

$$\phi\tau_{f12} = \partial_y(v_1 + \phi w_1), \tag{3.15b}$$

$$\phi\tau_{s12} = p_1 y - (1 - \phi)\tau_{f12}, \tag{3.15c}$$

$$\partial_y w_1 = \tau_{f12} - \frac{\tau_{s12}}{\eta_s(\phi)}, \tag{3.15d}$$

$$p_c = \eta_n(\phi)|\partial_y(v_1 - (1 - \phi)w_1)|. \tag{3.15e}$$

In the unyielded region $y \in [0; y_B[$, equations (3.15a)–(3.15c) stay the same, but the two remaining ones are replaced by

$$\partial_y(v_1 - (1 - \phi)w_1) = 0 \qquad \text{and} \qquad \phi = \phi_{\mathrm{sc}}, \tag{3.15f}$$

The boundary conditions are the no-slip

$$v_1 = 0, \quad w_1 = 0, \qquad \text{at } y = 1/2, \tag{3.15g}$$

and symmetry conditions

$$\partial_y v_1 = 0, \quad \partial_y w_1 = 0, \qquad \text{at } y = 0. \tag{3.15h}$$

In case the unyielded region fills up the whole channel, i.e., $y_B = 1/2$, the no-slip boundary conditions together with (3.15f) gives $v_1 - (1 - \phi)w_1 = 0$. Then, (3.15a) becomes the Brinkman equation, cf. [7]. For the yield surface at $y = y_B$, we demand the continuity conditions

$$[\tau_{s12}]_-^+ = 0, \qquad\qquad [\tau_{f12}]_-^+ = 0, \qquad\qquad [v_1]_-^+ = 0, \tag{3.15i}$$

$$[w_1]_-^+ = 0, \qquad\qquad [\phi]_-^+ = 0, \tag{3.15j}$$

where we denote $[g]_-^+ = \lim_{y \searrow y_B} g - \lim_{y \nearrow y_B} g$. We remark that these conditions are not all independent, as, for example, the second condition in (3.15h) can be obtained from the first via (3.15f), and the continuity of one of the stresses in (3.15j) implies the other via (3.15c).

Notice that (3.4c) applies in the region $[y_B; 1/2]$, where $\dot{\gamma}_s > 0$, so that if $y_B < 1/2$ (i.e., excluding the special case where the entire channel is jammed with $\phi = \phi_{\mathrm{sc}}$), then $p_c = 0$ implies $\phi = 0$.

Notice that if $p_c = 0$, then (3.4c) implies that $\phi = 0$ in the region $[y_B; 1/2]$. This would mean that all particles have moved to the unyielded region and, unless we are in the special case where $y_B = 1/2$ and hence $\phi = \phi_{\mathrm{sc}}$ everywhere, have left a clear liquid phase behind. This is unplausible and certainly not what is observed in experiments, e.g., in [22], and it is not the type of solution that arises from a homogeneous initial state in the time-dependent version of the equations discussed in Section 4.1, see Figure 5. We therefore assume $p_c > 0$. Then, we can remove p_c from the equations by rescaling

$$\tau_{s12} = p_c\tilde{\tau}_{s12}, \quad \tau_{f12} = p_c\tilde{\tau}_{s12}, \quad p_1 = p_c\tilde{p}_1, \quad v_1 = p_c\tilde{v}_1, \quad w_1 = p_c\tilde{w}_1. \tag{3.16}$$

The fact that p_c can be scaled out of the problem in this way implies that the width of the unyielded region i.e., y_B does not depend on p_c, as was reported in [25]. We note that in conventional Herschel–Bulkley models, which are also able to capture yield stress and shear-thinning, the unyielded region would change with p_c.

3.2 Phase space analysis

We now derive conditions for the existence of solutions to system (3.15). For this, it is convenient to reduce the system into a second order, non-autonomous system of ordinary differential equations for $w \equiv w_1$ and ϕ. For convenience, we also introduce the notation $u_f \equiv u_{f1} = v_1 + (1 - \phi)w_1$ and $u_s \equiv u_{s1} = v_1 - (1 - \phi)w_1$ for the first components of $\boldsymbol{u}_f$ and $\boldsymbol{u}_s$, respectively.

We first note that in the fluid region $y \in [y_B ; 1/2]$ combining the definition of the solid stress (3.4c) and (3.15e) yields

$$\phi\tau_{s12} = \phi\eta_s\partial_y u_s = \frac{\phi\eta_s}{\eta_n}\text{sign}(\partial_y u_s) = -\frac{\phi\eta_s}{\eta_n}\text{sign}(y), \tag{3.17}$$

Here, we have used that $\text{sign}(\partial_y u_s) = \text{sign}(\tau_{s12}) = -\text{sign}(y)$, where we recall that due to (3.14b) the total stress is just a linear function of y. Then, using (3.15c) in (3.15a) and (3.17) yields

$$\partial_y N(\phi) = -\phi p_1 + \text{Da}\frac{\phi^2}{1 - \phi}w, \tag{3.18a}$$

which will be used as an equation for the solid volume fraction. We get an equation for w by combining (3.15c) and (3.15d) to give

$$\partial_y w = \frac{p_1 y + N(\phi)}{1 - \phi} + \frac{1}{\eta_n(\phi)}. \tag{3.18b}$$

The function N is given by

$$N(\phi) \equiv \frac{\phi\eta_s(\phi)}{\eta_n(\phi)}.$$

In the unyielded region $y \in [0 ; y_B[$ we already know

$$\phi = \phi_{sc}, \tag{3.18c}$$

and since $\partial_y u_s = 0$, we have $\tau_{f12} = \partial_y u_f = \partial_y w$, which together with (3.15a) is

$$\partial_{yy} w = p_1 + \text{Da}\frac{\phi_{sc}^2}{(1 - \phi_{sc})^2}w. \tag{3.18d}$$

At the channel wall and centre, we have the boundary conditions

$$w = 0 \qquad\qquad \text{at } y = 1/2, \tag{3.18e}$$

$$\partial_y w = 0 \qquad\qquad \text{at } y = 0, \tag{3.18f}$$

and at the yield surface,

$$\phi = \phi_{\text{sc}}, \quad [w]_-^+ = 0, \quad [w_y]_-^+ = 0, \quad \text{at } y = y_B. \qquad (3.18g)$$

The problem for w in the unyielded region, (3.18*d*) and (3.18*f*), can now be solved explicitly. For Da > 0, we have

$$w = \alpha_1 \cosh\left(\frac{\text{Da}^{1/2}\phi_{\text{sc}}}{1 - \phi_{\text{sc}}}y\right) - \frac{(1 - \phi_{\text{sc}})^2}{\text{Da }\phi_{\text{sc}}^2}p_1, \qquad (3.19)$$

where α_1 is a constant of integration. We can use this in the last two conditions in (3.18*g*) to get

$$\partial_y w = \left(w + \frac{(1 - \phi_{\text{sc}})^2}{\text{Da }\phi_{\text{sc}}^2}p_1\right)\frac{\text{Da}^{1/2}\phi_{\text{sc}}}{1 - \phi_{\text{sc}}}\tanh\left(\frac{\text{Da}^{1/2}\phi_{\text{sc}}}{1 - \phi_{\text{sc}}}y_B\right), \quad \text{at } y = y_B, \qquad (3.20)$$

and from this a new formulation of the free-boundary condition

$$\phi = \phi_{\text{sc}}, \qquad (3.21a)$$

$$w = W(y_B) \equiv \frac{p_1 y_B + \mu_1}{\text{Da}^{1/2}\phi_{\text{sc}}\tanh\left(\frac{\text{Da}^{1/2}\phi_{\text{sc}}}{1 - \phi_{\text{sc}}}y_B\right)} - \frac{(1 - \phi_{\text{sc}})^2}{\text{Da }\phi_{\text{sc}}^2}p_1, \quad \text{at } y = y_B. \qquad (3.21b)$$

We have thus reduced the problem to a free-boundary value problem for a second-order system of ordinary differential equations (3.18*a*), (3.18*b*) with a condition (3.18*e*) at the fixed boundary and two at the free boundary (3.21*a*), (3.21*b*).

This free-boundary value problem contains the parameters Da, ϕ_{sc}, p_1, μ_1, μ_2, I_0. The critical volume fraction ϕ_{sc} is typically chosen between 0.63–0.68 (volume fraction at maximum random packing). The channel pressure gradient value p_1 will always be negative and for concentrated suspensions Da, which proportional $(L/a)^2$ is typically quite large, see e.g., [35, 37]. The three parameter μ_1, μ_2 and I_0 are material parameters. In our study, we fix

$$\phi_{\text{sc}} = 0.63, \qquad \mu_1 = 1, \qquad I_0 = 0.005, \qquad (3.22)$$

and vary p_1 and Da for μ_1 and μ_2.

For the solution of the boundary value problem (3.18), we proceed as follows. We solve (3.18*a*), (3.18*b*) as an initial value problem with initial values $\phi(1/2) = \phi_0$ and $w(1/2) = 0$ using e.g., Matlab's *ode*15*s* solver. The solution is followed for decreasing y until the volume fraction hits the value ϕ_{sc} or y reaches zero. The situation is shown for a range of ϕ_0 in Figure 2. It turns out that typically there is a value $0 < \phi^* < \phi_{\text{sc}}$ so that the former case happens for $\phi_0 \geqslant \phi^*$ and the latter if $\phi_0 < \phi^*$. We discard these values since only trajectories that intersect with $\phi = \phi_{\text{sc}}$ can lead to solutions of the boundary value problem (3.18). For the remaining ϕ_0 in the interval $[\phi^*, \phi_{\text{sc}}]$, we determine y_B and $w(y_B)$ and plot the curve $(y_B(\phi_0), w(y_B(\phi_0)))$ as we vary ϕ_0. The intersection of this curve with the graph of the function $W(y_B)$ (as defined in (3.21*b*)), shown in Figure 2 identifies the unique value for ϕ_0 that gives rise to a solution of (3.18). The corresponding trajectory
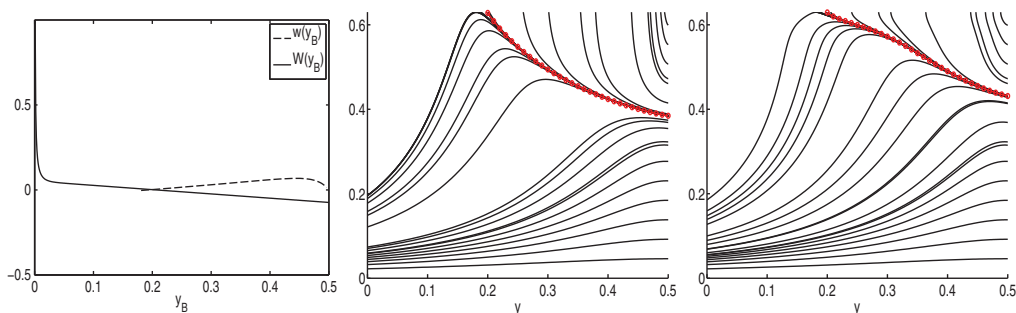
FIGURE 2. (left) The $w(y_B)$ solution curve together with the W-boundary condition and the projection of trajectories for (3.18a), (3.18b) onto the ϕ-y-plane with initial values $w = 0$, $\phi = \phi_0$ for a range of values. For the other parameters, we used $Da = 1{,}000$, $\mu_1 = \mu_2 = 1$ (middle) and $\mu_1 = 1$, $\mu_2 = 1.5$ (right), where the latter case shows the impact of the viscosity term (2.8e) proposed in Boyer *et al.* [5], which is zero for $\mu_1 = \mu_2$.

is the unique symmetric solution with a single unyielded region and its projection on the y-ϕ-plane in Figure 2 is emphasized by bullets.

We note that the solution of the boundary value problem (3.18), can also be obtained by rewriting (3.18a) for w, i.e.,

$$w = \frac{\left(\partial_y N + \phi\, p_1\right)\left(1 - \phi\right)}{Da\,\phi^2}, \tag{3.23}$$

and using it in (3.18b) and in the boundary conditions. This yields an equation solely in ϕ, i.e.,

$$\partial_y \left(\frac{\left(\partial_y N + \phi\, p_1\right)\left(1 - \phi\right)}{Da\,\phi^2} \right) = \frac{p_1 y + N}{1 - \phi} + \frac{1}{\eta_n}, \tag{3.24a}$$

with boundary conditions

$$0 = \partial_y N + \phi\, p_1 \qquad\qquad \text{at } y = \frac{1}{2}, \tag{3.24b}$$

$$\phi = \phi_{sc} \qquad\qquad \text{at } y = y_B, \tag{3.24c}$$

$$\frac{\left(\partial_y N + p_1\right)\left(1 - \phi_{sc}\right)}{Da\,\phi_{sc}{}^2} = \frac{p_1 y_B + \mu_1}{Da^{\frac{1}{2}}\phi_{sc}\tanh\left(\frac{Da^{\frac{1}{2}}\phi_{sc}}{1 - \phi_{sc}} y_B\right)} \qquad \text{at } y = y_B. \tag{3.24d}$$

We transform the free-boundary problem (3.24) into fixed-domain problem via

$$y = \left(y_B - \frac{1}{2}\right)\zeta + \frac{1}{2}, \tag{3.25}$$

where $\zeta \in [0, 1]$, which introduces the free-boundary coordinate as an explicit parameter in the system and then we add the trivial differential equation for the constant y_B to get
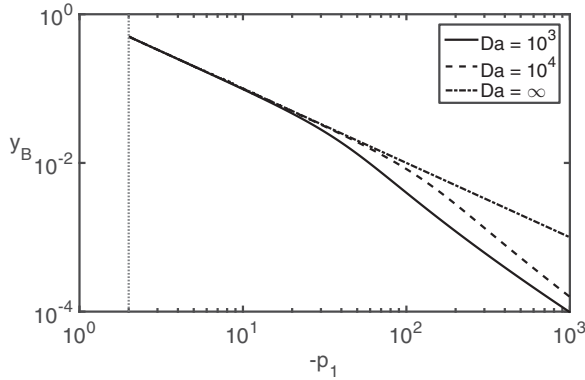
FIGURE 3. The dependence of the yield surface position y_B on the pressure gradient magnitude p_1, for parameters (3.22), $\mu_2 = 1$. The solid curve shows the results for Da $= 1,000$; the dashed curve for Da $= 10,000$; the dotted-dashed curve for Da $= \infty$. The dotted vertical line represents the minimum pressure gradient $p_{\min} \approx 2$, where the unyielded region fills the entire channel.

the boundary value problem

$$\frac{1}{y_B - \frac{1}{2}}\partial_\zeta \left(\frac{\left(\frac{1}{y_B-\frac{1}{2}}\partial_\zeta N + \phi\, p_1\right)(1-\phi)}{\mathrm{Da}\,\phi^2} \right) = \frac{p_1\left((y_B - \frac{1}{2})\zeta + \frac{1}{2}\right) + N}{1-\phi} + \frac{1}{\eta_n}, \quad (3.26a)$$

$$\partial_\zeta y_B = 0 \quad (3.26b)$$

with boundary conditions

$$0 = \partial_\zeta N + \left(y_B - \frac{1}{2}\right)\phi\, p_1 \qquad\qquad \text{at } \zeta = 0, \quad (3.26c)$$

$$\phi = \phi_{sc} \qquad\qquad \text{at } \zeta = 1, \quad (3.26d)$$

$$\partial_\zeta \phi = -\frac{2(y_B - \frac{1}{2})}{5(1-\phi_{sc})}\frac{\mathrm{Da}^{\frac{1}{2}}\phi_{sc}(p_1 y_B + \mu_1)}{\tanh\left(\frac{\mathrm{Da}^{\frac{1}{2}}\phi_{sc}}{1-\phi_{sc}}y_B\right)} + \frac{2}{5}\left(y_B - \frac{1}{2}\right)p_1 \qquad \text{at } \zeta = 1. \quad (3.26e)$$

After solving for ϕ, we can determine the remaining variables by first using (3.23) for w, next solving for $(1-\phi)\tau_{f12}$ via (3.15a) with $((1-\phi)\tau_{f12})(0) = 0$ and then get the fluid velocity via (3.15e) with $u_f(1/2) = 0$. The solid variables are then easily computable by (3.15c) and $u_s = u_f - w$.

The dependence of the width of the unyielded zone on the pressure gradient is shown in Figure 3. As the magnitude of the pressure gradient $-p_1$ decreases, the thickness of the unyielded zone increases until the interface between the yielded and unyielded zones reaches the wall, that is, $y_B = 1/2$, for $-p_1 \leqslant p_{\min}$. Setting $y = 1/2$ in (3.21b) and solving for p_1 gives an explicit expression for this minimum pressure,

$$p_{\min} = \frac{\phi_{sc}\mathrm{Da}\,\mu_1}{\tanh\left(\frac{\sqrt{\mathrm{Da}}\,\phi_{sc}}{2(\phi_{sc}-1)}\right)\sqrt{\mathrm{Da}}\,(1-\phi_{sc})^2 + \mathrm{Da}\,\phi_{sc}/2}, \quad (3.27)$$

below which the solid phase is jammed in the entire cross-section of the channel. On the other hand, for $-p_1 > p_{\min}$ the phase plane analysis suggests that there is always a unique and strictly positive value for y_B, which moreover tends to zero as $p_1 \to -\infty$. We also note that for large Da and fixed p_1, the interface position tends to a finite value,

$$y_B \to -\frac{\mu_1}{p_1}. \tag{3.28}$$

Remark. For a finite length channel, the two free parameters p_1 and p_c in the solution for the solid fraction ϕ_s and for the velocity profiles u_s and u_f are typically fixed by, e.g., inlet conditions for the solid and liquid fluxes. Notice that here we are reverting to the original parameter p_1 prior to the rescaling in (3.16). Mass conservation dictates that for each phase, the total fluxes must be constant along the channel, thus we have the conditions

$$2p_c \int_0^{1/2} (1 - \phi(y; p_1/p_c))u_f(y; p_1/p_c)dy = \frac{1 - \phi_{in}}{6}, \tag{3.29a}$$

$$2p_c \int_0^{1/2} \phi(y; p_1/p_c)u_s(y; p_1/p_c)dy = \frac{\phi_{in}u_{s,in}}{6}, \tag{3.29b}$$

where ϕ_{in} and $u_{s,in}$ are the solid phase volume fraction and the scaling factor for the parabolic solid phase velocity profile assumed at the inlet (see (3.1)). Also, recall that $u_{f,in} = 1$ by our choice of the velocity scale. From our previous investigation, we know that the flow will always produce a plug in the centre where the solid phase is jammed, that is, $\phi = \phi_{sc}$. This is possible by having a solid phase profile that is equal to ϕ_{sc} only in a very narrow region at the centre of the channel and then rapidly decays to zero towards the walls. Thus, the total solid flux through the cross-section can be arbitrarily small. For such solutions, however, finite size effects may come into play that are neglected in the continuum model.

3.3 Asymptotic analysis for large Da

The stationary solutions show that the solid volume fraction increases towards the channel centre, where a finite size region at maximum packing is located, see Figure 4. The solid phase velocity increases towards the centre but is constant in the region where $\phi = \phi_{sc}$, so that there, the solid phase is jammed, or unyielded and effectively forms a porous medium. The fluid velocity increases at first but then decreases towards the centre of the channel, where it has a local minimum. The difference between the two velocities achieves a maximum away from the jammed region. Moreover, for growing Da the solution of the stationary problem develops boundary layers, in particular the velocity w shows a pronounced sharp drop as y approaches the boundary $y = 1/2$. In addition, as Da increases, the velocity difference w decreases by approximately the same factor. This observation and the large values of Da suggest that we seek and asymptotic approximation in the limit $\varepsilon \equiv 1/\text{Da} \to 0$ with the ansatz $w = \varepsilon\tilde{w}$. The asymptotic analysis of the stationary solution will yield the key ideas for the derivation of a new drift-flux model from the time-dependent two-phase flow model for concentrated
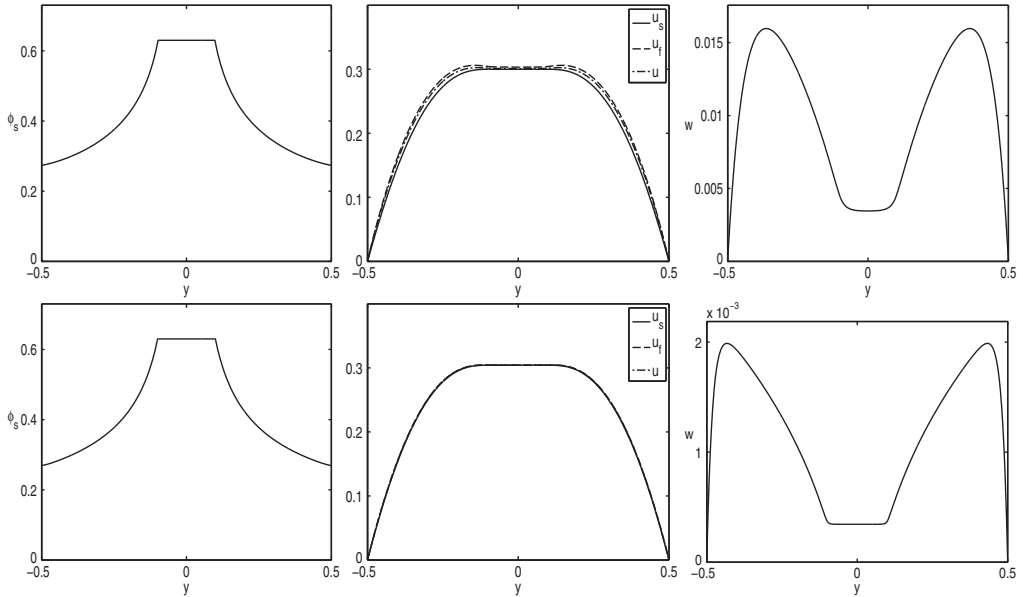
FIGURE 4. (left) The solid volume fraction ϕ, (middle) the velocities $\boldsymbol{u}_s, \boldsymbol{u}_f, \boldsymbol{u}$ and (right) the velocity difference w obtained by using the ODE problem (3.18). The parameters are given by (3.22), $\mu_2 = 1$, and $p_1 = -10$. Top figures show results for Da $= 1,000$ and bottom figures for Da $= 10,000$.

suspensions, which we then use to study the formation and evolution of jammed regions in the flow.

For the remaining analysis, we drop the tilde and obtain from (3.18a)

$$w = p_1 \frac{1-\phi}{\phi} + \frac{1-\phi}{\phi^2} N'(\phi)\partial_y\phi. \tag{3.30a}$$

Substitution the rescaled version of (3.18b) yields a second-order equation for ϕ,

$$\varepsilon \, \partial_y \left(p_1 \frac{1-\phi}{\phi} + \frac{1-\phi}{\phi^2} N'(\phi)\partial_y\phi \right) = \frac{p_1 y + N(\phi)}{1-\phi} + \frac{(\phi_{sc} - \phi)^2}{\phi^2}. \tag{3.30b}$$

The boundary conditions at the yield interface $y = y_B$ are

$$\phi = \phi_{sc}, \tag{3.30c}$$

$$\partial_y\phi = -\frac{2}{5} \frac{\phi_{sc}}{1-\phi_{sc}} \frac{p_1 y_B + \mu_1}{\tanh\left(\frac{\phi_{sc}}{1-\phi_{sc}}\varepsilon^{-1/2}y_B\right)} \varepsilon^{-1/2} + \frac{2}{5}p_1, \tag{3.30d}$$

and at the channel wall we have $w = 0$, so that from (3.30a), we get

$$\partial_y\phi = -p_1 \frac{\phi}{N'(\phi)} \quad \text{at } y = \frac{1}{2}. \tag{3.30e}$$

Clearly, this is a singular perturbed problem with a boundary layer at $y = 1/2$ and $y = y_B$.

In fact, if we assume that ϕ and y_B have asymptotic expansions

$$\phi(y) = \phi_0(y) + \varepsilon^{1/2}\phi_1(y) + O(\varepsilon), \qquad y_B = y_{B0} + \varepsilon\, y_{B1} + O(\varepsilon^2). \tag{3.31}$$

Then to leading order we have

$$0 = \frac{p_1 y + N(\phi_0)}{1 - \phi_0} + \frac{(\phi_{\mathrm{sc}} - \phi_0)^2}{\phi_0^2}. \tag{3.32}$$

When we use this in (3.30a) the boundary conditions for w are not satisfied.

3.3.1 *Boundary layer problem at $y = 1/2$*

For the boundary layer variables $z = (\frac{1}{2} - y)\varepsilon^{-1/2}$ and $\Phi(z) = \phi(y)$ the governing equation is

$$\partial_z\left(-\varepsilon^{1/2}\, p_1 \frac{1 - \Phi}{\Phi} + \frac{1 - \Phi}{\Phi^2} N'(\Phi)\partial_z \Phi\right) = \frac{p_1/2 + N(\Phi) - \varepsilon^{1/2}\, z}{1 - \Phi} + \frac{(\phi_{\mathrm{sc}} - \Phi)^2}{\Phi^2}, \tag{3.33a}$$

with boundary condition at $z = 0$

$$(1 - \Phi)\, N'(\Phi)\, \partial_z \Phi = \varepsilon^{1/2}\, p_1\, (1 - \Phi)\Phi. \tag{3.33b}$$

Assume the asymptotic expansion of the inner variables can be written as

$$\Phi(z) = \Phi_0(z) + \varepsilon^{1/2}\Phi_1(z) + O(\varepsilon), \tag{3.34}$$

so that the solution satisfies to leading order the problem

$$\partial_z\left(\frac{1 - \Phi_0}{\Phi_0^2}\, N'(\Phi_0)\, \partial_z \Phi_0\right) = \frac{p_1/2 + N(\Phi_0)}{1 - \Phi_0} + \frac{(\phi_{\mathrm{sc}} - \Phi_0)^2}{\Phi_0^2}, \tag{3.35a}$$

$$\partial_z \Phi_0 = 0 \qquad \text{at} \quad z = 0^+, \tag{3.35b}$$

since $(1 - \Phi_0)\, N'(\Phi_0) \neq 0$. As $z \to \infty$ the solution approaches a constant, say $\Phi_0 \to \Phi_{0,\infty}$, which satisfies

$$\frac{p_1/2 + N(\Phi_{0,\infty})}{1 - \Phi_{0,\infty}} + \frac{(\phi_{\mathrm{sc}} - \Phi_{0,\infty})^2}{\Phi_{0,\infty}^2} = 0. \tag{3.36}$$

Hence, since for $y \to (1/2)^-$ in the leading order outer problem, then

$$0 = \frac{p_1/2 + N\big(\phi_0(1/2)\big)}{1 - \phi_0(1/2)} + \frac{\big(\phi_{\mathrm{sc}} - \phi_0(1/2)\big)^2}{\phi_0^2(1/2)}. \tag{3.37}$$

Therefore, matching yields $\Phi_{0,\infty} = \phi_0(1/2)$.

It is straightforward to solve the next order problem to obtain

$$\Phi_1(z) = \frac{A_2 N'(\phi_0(1/2)) - p_1 \phi_0(1/2) A_1}{A_1^{3/2} N'(\phi_0(1/2))} \exp\left(-\sqrt{A_1}z\right) + \frac{A_2}{A_1}z, \tag{3.38}$$

where

$$A_1 = \frac{\phi_0^2(1/2)}{(1 - \phi_0(1/2))^2} + \frac{\phi_0^2(1/2)}{N'(\phi_0(1/2))} \frac{\frac{1}{2}p_1 + N(\phi_0(1/2))}{(1 - \phi_0(1/2))^3}$$
$$- \frac{2}{N'(\phi_0(1/2))} \frac{\phi_{sc}}{\phi_0(1/2)} \frac{\phi_{sc} - \phi_0(1/2)}{1 - \phi_0(1/2)}, \tag{3.39a}$$

$$A_2 = \frac{p_1}{N'(\phi_0(1/2))} \frac{\phi_0^2(1/2)}{(1 - \phi_0(1/2))^2}, \tag{3.39b}$$

thus, using (3.37)

$$\frac{A_2}{A_1} = p_1 \left[N'(\phi_0(1/2)) + \frac{(\phi_{sc} - \phi_0(1/2))(\phi_0^2(1/2) - 2\phi_{sc} + \phi_{sc}\phi_0(1/2))}{\phi_0^3(1/2)} \right]^{-1}. \tag{3.40}$$

Taking the y-derivative of (3.32), we get

$$\partial_y \phi_0 = -p_1 \left[N'(\phi_0) + \frac{\phi_{sc} - \phi_0}{\phi_0^3} (\phi_0^2 - 2\phi_{sc} + \phi_0\phi_{sc}) \right]^{-1}. \tag{3.41}$$

Therefore, the linear term in the expansion of the outer solution ϕ_0 and in the inner solution Φ_1, see (3.38), match as required.

3.3.2 *Boundary layer problem at $y = y_B$*

Similarly, we let the boundary layer variables be

$$\xi = \frac{y - y_B}{\varepsilon^{1/2}}, \qquad \varphi(\xi) = \phi(y). \tag{3.42}$$

To leading order the problem now reads

$$\partial_\xi \left(\frac{1 - \varphi_0}{\varphi_0^2} N'(\varphi_0) \partial_\xi \varphi_0 \right) = \frac{p_1 y_{B0} + N(\varphi_0)}{1 - \varphi_0} + \frac{(\phi_{sc} - \varphi_0)^2}{\varphi_0^2}, \tag{3.43a}$$

with boundary condition at $\xi = 0^+$

$$\varphi_0(0) = \phi_{sc}, \tag{3.43b}$$

and

$$\partial_\xi \varphi_0(0) = -\frac{2}{5} \frac{\phi_{sc}}{1 - \phi_{sc}} (p_1 y_{B0} + \mu_1) = 0. \tag{3.43c}$$

Note, if we assume that in the leading order outer equation, ϕ also satisfies $\phi = \phi_{sc}$ at $y = y_B$ then we must have that $p_1 y_{B0} + \mu_1 = 0$, since $N(\phi_{sc}) = \mu_1$. Hence, the second

boundary condition is also zero. This suggests $\varphi_0 = \phi_{sc}$. Matching this to the leading order outer problem

$$\frac{p_1\, y_{B0} + N(\phi_0(y_{B0}))}{1 - \phi_0(y_B)} + \frac{(\phi_{sc} - \phi_0(y_B))^2}{\phi_0^2(y_B)} = 0. \tag{3.44}$$

Hence, $\phi_0(y_B) = \phi_{sc}$. Solving the next order problem

$$\partial_{\xi\xi}\varphi_1 = \left(\varphi_1 - \frac{2}{5}\,p_1\,\xi\right)\frac{\phi_{sc}{}^2}{(1 - \phi_{sc})^2}, \tag{3.45a}$$

with boundary conditions

$$\varphi_1(0) = 0, \quad \partial_\xi\varphi_1(0) = \frac{2}{5}\,p_1, \tag{3.45b}$$

gives

$$\varphi_1(\xi) = \frac{2}{5}p_1\xi. \tag{3.46}$$

This needs to be matched with the linear term in the Taylor expansion of the leading order outer solution ϕ_0, which can be obtained by taking the limit $\phi \to \phi_{sc}$ in (3.41). That limit gives $\partial_y\phi_0(y_B) = -p_1/N'(\phi_{sc}) = -p_1/(-5/2)$, that is, the coefficients are equal, hence the terms match.

4 Drift-flux model for plane Poiseuille flow

While drift-flux models have been proposed to study the evolution of two-phase flows of suspensions [31, 39] and are also used as transport equations for a suspended phase and combined with hydrodynamic equations [11, 36] a systematic asymptotic derivation from the underlying two-phase model is still open. Here, we will use matched asymptotics along the lines of the analysis of the stationary problem, for the derivation of a new drift-flux model for the cross-sectional flow of the channel. Our analysis shows that the inclusion of the boundary layers leads to a drift-flux model that naturally accounts for the shear-induced flux of the suspended phase away from the boundaries. Moreover, the constitutive law for concentrated suspensions leads to the appearance of unyielded and yielded regions, which needs to be captured by the new drift-flux model.

4.1 Asymptotic derivation of the drift-flux model

To capture the evolution towards a Bingham-type flow, it will be instructive to investigate the problem for the cross-section. We assume therefore that all the variables depend only on y and t, except for the pressure variables, which also depend on x.

As in our previous section, the drift-flux regime is established for large Da and small velocity differences w, and in addition on a long-time scale. Hence, we let $\varepsilon = 1/\text{Da}$ and

$$w_1 = \varepsilon w_1^*, \quad w_2 = \varepsilon w_2^*, \quad t = \frac{t^*}{\varepsilon}. \tag{4.1}$$

The governing equations are then, after we drop the '∗'

$$\partial_t \phi - \partial_y(\phi(1 - \phi)w_2) = 0, \tag{4.2a}$$

$$-\partial_y \left[(1 - \phi)\partial_y v_1 + \varepsilon(1 - \phi)\partial_y(\phi w_1)\right] + (1 - \phi)\partial_x p_f = -\frac{\phi^2}{1 - \phi}w_1, \tag{4.2b}$$

$$-\partial_y \left[2\varepsilon(1 - \phi)\partial_y(\phi w_2)\right] + (1 - \phi)\partial_y p_f = -\frac{\phi^2}{1 - \phi}w_2, \tag{4.2c}$$

$$-\partial_y \left[\phi\eta_s\partial_y v_1 - \varepsilon\phi\eta_s\partial_y((1 - \phi)w_1)\right] + \phi\partial_x p_f = \frac{\phi^2}{1 - \phi}w_1, \tag{4.2d}$$

$$\partial_y \left[2\varepsilon\phi\,\partial_y((1 - \phi)w_2)\right] + \phi\partial_y p_f + \partial_y p_c = \frac{\phi^2}{1 - \phi}w_2, \tag{4.2e}$$

$$p_c = \eta_n(\phi) \left[(\partial_y v_1 - \varepsilon\partial_y((1 - \phi)w_1))^2 + 2\varepsilon[\partial_y((1 - \phi)w_2)]^2\right]^{1/2} + \varepsilon^4\phi, \tag{4.2f}$$

and no-slip conditions at $y = \pm 1/2$

$$v_1 = 0, \quad w_1 = 0, \quad w_2 = 0. \tag{4.2g}$$

To leading order, we obtain for the outer problem

$$\partial_t \phi - \partial_y(\phi(1 - \phi)w_2) = 0, \tag{4.3a}$$

$$-\partial_y[(1 - \phi)\partial_y v_1] + (1 - \phi)\partial_x p_f = -\frac{\phi^2}{1 - \phi}w_1, \tag{4.3b}$$

$$(1 - \phi)\partial_y p_f = -\frac{\phi^2}{1 - \phi}w_2, \tag{4.3c}$$

$$-\partial_y[\phi\eta_s\partial_y v_1] + \phi\partial_x p_f + \partial_x p_c = \frac{\phi^2}{1 - \phi}w_1, \tag{4.3d}$$

$$\phi\partial_y p_f + \partial_y p_c = \frac{\phi^2}{1 - \phi}w_2, \tag{4.3e}$$

$$p_c = \eta_n |\partial_y v_1|, \tag{4.3f}$$

and no-slip conditions at $y = \pm 1/2$,

$$v_1 = 0, \quad w_1 = 0, \quad w_2 = 0. \tag{4.3g}$$

We note that for ease of notation, we have dropped the indices in the variables that denote the leading order solutions. Adding (4.3c) and (4.3e) yields $\partial_y(p_f + p_c) = 0$, hence $p_f + p_c = f(x)$. Adding (4.3b) and (4.3d) yields

$$-\partial_y \left([\phi\eta_s + (1 - \phi)]\,\partial_y v_1\right) + \partial_x(p_f + p_c) = 0. \tag{4.4}$$

Since the left-hand side is only dependent on y and the right-hand side only on x, they must be constants. Thus, defining $\partial_x(p_f + p_c) = p_2$, so that after integration

$$[\phi\eta_s + (1 - \phi)]\,\partial_y v_1 = p_2 y + \alpha. \tag{4.5}$$

Adding $(1 - \phi)\partial_y p_c$ on both sides of (4.3c) yields

$$\partial_y p_c = \frac{\phi^2}{(1 - \phi)^2} w_2. \qquad (4.6)$$

We have

$$w_2 = \frac{(1 - \phi)^2}{\phi^2} \partial_y \left(\eta_n |\partial_y v_1| \right) = \frac{(1 - \phi)^2}{\phi^2} \partial_y \left(\eta_n \dot{\gamma} \right). \qquad (4.7)$$

In addition note that from (4.5), we obtain

$$\partial_y v_1 = \frac{p_2 \, y}{\phi \eta_s + 1 - \phi}, \qquad (4.8)$$

where due to symmetry we have set $\alpha = 0$. Since $p_2 < 0$ the negative of this expression will always be positive and we set

$$\dot{\gamma} = -\frac{p_2 \, y}{\phi \eta_s + 1 - \phi}, \qquad (4.9)$$

so that

$$w_2 = -p_2 \frac{(1 - \phi)^2}{\phi^2} \partial_y \left[\frac{\eta_n y}{\phi \eta_s + 1 - \phi} \right]. \qquad (4.10)$$

Hence, we obtain for the drift-flux model

$$\partial_t \phi = -p_2 \partial_y \left[\frac{(1 - \phi)^3}{\phi} \partial_y \left(\frac{y}{N(\phi) + \frac{1 - \phi}{\eta_n(\phi)}} \right) \right]. \qquad (4.11)$$

We note at this point that the drift-flux model we have just derived (4.11) is a non-linear diffusion equation that admits constant solutions, say ϕ_0. Linearizing about these base states by making the ansatz $\phi(t, y) = \phi_0 + \delta \, \phi_1(t, y) + O(\delta^2)$, we obtain to $O(\delta)$

$$\partial_t \phi_1 = -p_2 \, \partial_y \left[\frac{M'(\phi_0)}{F(\phi_0)} \phi_1 - M(\phi_0) \frac{F'(\phi_0)}{F^2(\phi_0)} \partial_y (y \phi_1) \right], \qquad (4.12)$$

where $M(\phi) = (1 - \phi)^3/\phi$ and $F(\phi) = N(\phi) + (1 - \phi)/\eta_n(\phi)$. We supplement this equation with boundary conditions and assume no-flux conditions at the wall $y = 1/2$. Indeed, as shown in Appendix B, matching to a boundary layer there gives $w_2 = 0$. We seek solutions that are symmetric with respect to the middle axis of the channel, thus we also impose $w_2 = 0$ at $y = 0$.

Clearly, if $F'(\phi_0) < 0$, which holds true for all $\phi_0 \in [0, \phi_{sc}]$ as long as $\mu_2 \geqslant \mu_1$ and $I_0 \geqslant 0$, then any perturbation of the constant base states is damped out and the flow remains. But we note that non-zero constant solutions of (4.11) do not satisfy the boundary conditions. Hence, we expect a non-linear structure to arise from the interplay between the drift-flux equation and the no-flux condition. Indeed, the flux of the solid phase leads to an increase of ϕ at the centre of the channel, until the solid volume fraction reaches ϕ_{sc} there and jamming of the solid phase occurs in a region $y < y_B$ with a time-dependent free boundary $y_B(t)$. In fact, $w_2 = 0$ cannot be achieved by the channel centre $y = 0$ at the right-hand side of (4.10), thus the jammed region emerges instantaneously, that is,

$y_B(t) > 0$ for all $t > 0$. In the jammed region, the solid volume fraction is constant so that mass conservation gives $w_2 = w_2(t)$. Assuming symmetry at $y = 0$ then fixes w_2 to be zero to all orders in ε for $0 < y < y_B$. At $y = y_B$, we therefore impose $\phi = \phi_{sc}$ and $w_2 = 0$, so that we have two boundary conditions as required at a free boundary. Figure 5 shows a numerical solution for the drift-flux model (4.11) with

$$\partial_y \left(\frac{y}{N(\phi) + \frac{1-\phi}{\eta_n(\phi)}} \right) = 0 \tag{4.13}$$

imposed at $y = 1/2$ and at $y = y_B$. The second condition

$$\phi = \phi_{sc} \quad \text{at } y = y_B, \tag{4.14}$$

is used to update the free boundary y_B. A central finite difference scheme of second order with a fully implicit Euler–Euler-2-step method was used to discretize the problem. The results in Figure 5 clearly display the emergence and evolution of the jammed region in the cross-sectional channel flow.

The evolution eventually tends to a stationary state that can be obtained from (4.11) by letting $\partial_t \phi = 0$. Integrating once and using (4.13) at $y = 1/2$ and then integrating once again leads to

$$\frac{y}{N(\phi) + \frac{1-\phi}{\eta_n(\phi)}} = c_1. \tag{4.15}$$

With $c_1 = -1/p_1$, we recover the stationary outer equation (3.32) from Section 3. Its value is fixed here by the requirement that the total amount of solid phase material

$$V_s = \int_0^{1/2} \phi \, dy, \tag{4.16}$$

is equal to the total amount present in the initial condition $\phi(y, 0)$ for the time-dependent problem. This follows from the observation that V_s is a conserved quantity for the time-dependent problem. The corresponding solution is indicated in the figure by open circles. It agrees well with the long-time profile for ϕ obtained from the time-dependent problem.

Remark. Before we continue with our analysis, we like to note that it is well-known that the non-viscous one-pressure two-fluid system contains an ill-posedness, that manifests itself in the occurrence of complex characteristics in the system and a subsequent loss of hyperbolicity in time, see also the recent discussion in [32]. The problem exists even for models that include viscous terms [40]. Although there has been progress towards a mathematical understanding during the last decade, see, e.g., [29] and references therein, until now there is no consistent and at the same time physically meaningful approach that resolves this problem. For the model above, we propose a mathematically motivated regularization to avoid the problem of loss of hyperbolicity. If we introduce a modified expression for the collision pressure of the form

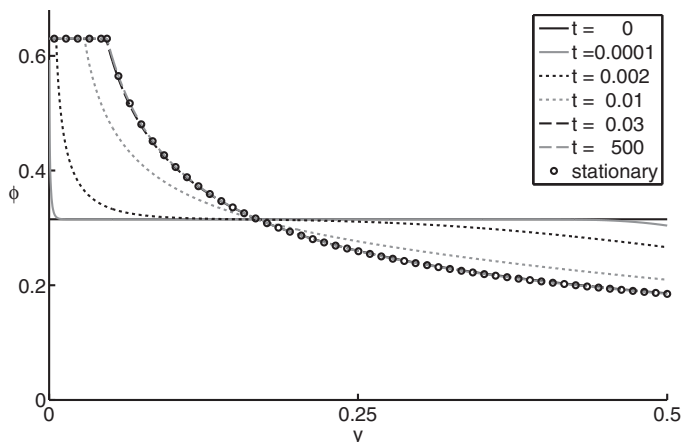$$p_c = \eta_n(\phi)|\dot{\gamma}_s| + c\phi, \tag{4.17}$$

FIGURE 5. Time evolution of solid volume fraction using the outer drift-flux approximation (4.11) for the parameters from (3.22) with $\mu_1 = \mu_2$ and $p_1 = -10$, starting from an initial uniform profile of $\phi(0, y) = \phi_{\text{sc}}/2$. The profile first changes near the channel centre and wall. The volume fraction increases near the centre until maximum packing is reached, which spawns an unyielded region. This unyielded region then grows so that y_B approaches the stationary value obtained from (3.28) and y converges to the stationary solution.

where c is a constant regularization parameter that is only slightly larger than

$$c_m = \frac{(u_f - u_s)^2}{\text{Da}^2}, \tag{4.18}$$

then the equation is hyperbolic i.e., all characteristics are real [32], but the additional term does not interfere with the derivation of the drift-flux model for $\text{Da} \gg 1$.

5 Discussion and outlook

In this study, we systematically derived a new two-phase model through ensemble averaging along the lines of Drew *et al.* [17] while incorporating recent non-Brownian constitutive laws by Boyer *et al.* [5] for the shear and normal viscosities for concentrated suspensions. Our study of plane Poiseuille flow using the two-phase model shows that solutions of this model naturally give rise to unyielded or jammed regions centred at the axis of symmetry for the channel. The width of such a region depends on the value of the applied pressure for a given volume fraction of the solid phase.

The parameter Da that appears in the model is typically very large because of small particle sizes. We use this here to derive a new drift-flux model that captures the shear-induced particle drift across the channel towards the centre and the format of a jammed region in the solution. The model also predicts that the particle drift across the pipe is by $O(1/\text{Da})$ smaller than the average flow along the channel. Our numerical results for the time-dependent drift-flux model reveal how the jammed region emerges first at the centre and then expands until the stationary state is reached. It would be interesting to relate this evolution to experimental results on the transition length over which a steady state develops in space from homogeneous inlet conditions.

At this point, it seems sensible to summarize the assumptions that underlie our model. While the general framework is based on the averaging of a microscopic model, much in the spirit of Drew [14], the non-linear nature of the microscopic equations requires additional constitutive laws for the macroscopic variables to obtain closure. The most important of these here is the stress–strain relation for the solid (i.e., particulate) phase (3.4b) and (3.4c). The justification of this law is based on the experiments by Boyer *et al.* [5], which clearly demonstrate the power law behaviour of η_n near a critical packing fraction and the presence of a yield stress that depends on the pressure excercized on the solid phase of the suspension. These experiments use a modified conical viscosimeter with a perforated surface so that pressure can be applied to the particles only, while permitting the liquid to leave or enter the suspension. A motion of the mixture is only achieved if a certain minimal torque is applied that increases with the applied pressure. Since the flow situation studied there is of Couette type with both phases moving at the same speed, our generalization needs to make a decision how to generalize the constitutive law to a situation where the relative speed is non-zero, and we resolve this here by applying the empirical law in Boyer *et al.* [5] to the solid phase only, while the liquid phase remains Newtonian.

A key aim of our paper is then to study the implications of such a law for Poiseuille flow as the simplest flow with spatially varying strain rate, and in particular address the important question if the pressure dependent yield stress leads to the formation of a plug similar to single-phase fluids. This is indeed the case for the solid phase, where a jammed region is formed, while the liquid is allowed to move relative to the solid phase. The strain rate dependence of the collision pressure and the decrease of the strain rate away from the channel walls impart a drift to the particles that leads to a net flux towards the channel centre in a homogeneous particle distribution. In the equilibrium density distribution, the density increases just enough to compensate the effect and leading to a zero pressure cross-flow gradient of the collision pressure and hence zero net flux. However, for the constitutive law considered here, the density profile reaches the critical volume fraction before the channel centre, and the solid phase jams.

An explanation for the occurrence of shear induced migration in connection with the drift-flux models was given in [31], see also [37, 39]. There, shear induced migration is the result of two effects, first, a spatially varying interaction frequency and second, of the spatially varying viscosity. If we consider only the first contribution, the key observation is that if the strain rate varies spatially over the typical size of a particle, then the collision frequency, which is given by the particle density times the strain rate, decreases over the cross-section of a particle in directions where the density is uniform but the strain rate decreases. This gradient in the collision frequency creates a flux of particles towards the region of lower strain rate. This picture holds up to particles located at the edge of a jammed region. Inclusion of the second effect results in a very similar condition, where the strain rate times a monotone function of the particle density has to be constant in steady state, which is exactly what we obtain from our drift-flux model if we set $w_2 = 0$ in (4.6) and use (4.3f). Thus, the particle distribution evolves into a non-uniform steady state, which, for our model, creates a jammed region at the centre of the channel as shown in Figure 5.

In any case, the prediction of a jammed region provides scope for further investigation. For example, such a region should be suppressed for smaller average solid volume fraction.

While our results show that the region decreases for less concentrated suspensions, it is always finite as long as a solid phase fraction is present at all. Even for very dense suspension, it is conceivable that the plug region is in a state where the particles are still permitted to have a small relative motion. In fact, previous modelling efforts using two-phase averaged models (or suspension balance models) have introduced various types of non-local terms to prevent the maximum solid volume fraction from being reached, especially in cases where a cusp forms at the centre line of pipe or channel flow, see, e.g., [33, 37], while others have not [53].

Moreover, the role of friction, as the solid volume fraction increases, needs to be considered more closely [13, 23, 51], to fully understand the physics that underly the transitions into the jammed state. Further insight into this could come from more experimental investigations, such as [38, 46] and the recent study [27], but also a more detailed understanding of the microscopic force balance in the concentrated suspension at the yield surface.

On the other hand, the derivation of the drift-flux model from the full two-phase model presented here could be extended further. The fact that the shear-induced particle transport acts on a different velocity scale than the phase-averaged flow field indicates how to systematically develop an asymptotic theory leading to a complete coupled flow model that includes both transport and jamming of particles. Such an analysis could also rationalize some suspension flow models that are found in the literature. In fact, the methods presented in this study should also enable the systematic derivation of drift-flux models for more complex flow geometries, for example, at the free boundary between the suspension and the surrounding atmosphere, or non-Newtonian carrier fluids [24], and will be part of our future work.

Finally, questions such as stability of dense suspension flows are rarely considered; for the model we develop here, a first step in this direction can be found in [3].

Acknowledgements

References

[1] AHMADPOUR, A. & SADEGHY, K. (2013) An exact solution for laminar, unidirectional flow of Houska thixotropic fluids in a circular pipe. *J. Non-Newton. Fluid Mech.* **194**, 23–31.

[2] AHNERT, T. (2015) *Mathematical Modeling of Concentrated Suspensions: Multiscale Analysis and Numerical Solutions.* PhD Thesis, Technical University Berlin, November.

[3] AHNERT, T., MÜNCH, A., NIETHAMMER, B. & WAGNER, B. (2018) Stability of concentrated suspensions under Couette and Poiseuille flow. *J. Eng. Math.* 1–27. https://doi.org/10.1007/s10665-018-9954-x

[4] BATCHELOR, G. K. & GREEN, J. T. (1972) The determination of the bulk stress in a suspension of spherical particles to order c^2. *J. Fluid Mech.* **56**(03), 401–427.

[5] BOYER, F., GUAZZELLI, É. & POULIQUEN, O. (2011) Unifying suspension and granular rheology. *Phys. Rev. Lett.* **107**(18), 188301.

[6] BRENNEN, C. E. (2005) *Fundamentals of Multiphase Flow*, Cambridge University Press, New York.

[7] BRINKMAN, H. C. (1949) A calculation of the viscous force exerted by a flowing fluid on a dense swarm of particles. *Appl. Sci. Res.* **1**(1), 27–34.

[8] CARTELLIER, A., ANDREOTTI, M. & SECHET, P. (2009) Induced agitation in homogeneous bubbly flows at moderate particle Reynolds number. *Phys. Rev. E* **80**(6).

[9] CASSAR, C., NICOLAS, M. & POULIQUEN, O. (2005) Submarine granular flows down inclined planes. *Phys. Fluids* **17**(10), 103301.

[10] W. CHOW, A., SINTON, S. W., IWAMIYA, J. H. & STEPHENS, T. S. (1994) Shear-induced particle migration in Couette and parallel-plate viscometers: NMR imaging and stress measurements. *Phys. Fluids* **6**(8), 2561–2576.

[11] COOK, B. P., BERTOZZI, A. L. & HOSOI, A. E. (2008) Shock solutions for particle-laden thin films. *SIAM J. Appl. Math.* **68**(3), 760–783.

[12] DE BRUYN, J. (2011) Unifying liquid and granular flow. *Physics* **4**, 86.

[13] DEGIULI, E., DÜRING, G., LERNER, E. & WYART, M. (2015) Unified theory of inertial granular flows and non-Brownian suspensions. *Phys. Rev. E* **91**(6), 062206.

[14] DREW, D. A. (1983) Mathematical modeling of two-phase flow. *Annu. Rev. Fluid Mech.* **15**(1), 261–291.

[15] DREW, D. A. (2001) A turbulent dispersion model for particles or bubbles. *J. Eng. Math.* **41**(2–3), 259–274.

[16] D. A. DREW & PASSMAN, S. L. (1999 *Theory of Multicomponent Fluids*, Applied Mathematical Sciences, Vol. 135, Springer, New York.

[17] DREW, D. A. & SEGEL, L. A. (1971) Averaged equations for two-phase media. *Stud. Appl. Math.* **50**(2), 205–231.

[18] EINSTEIN, A. (1906) Eine neue Bestimmung der Moleküldimensionen. *Ann. Phys.* **324**(2), 289–306.

[19] FOX, R. O. (2014) On multiphase turbulence models for collisional fluid-particle flows. *J. Fluid Mech.* **742**, 368–424.

[20] GADALAMARIA, F. & ACRIVOS, A. (1980) Shear-induced structure in a concentrated suspension of solid spheres. *J. Rheol.* **24**(6), 799–814.

[21] GARRIDO, P., CONCHA, F. & BÜRGER, R. (2003) Settling velocities of particulate systems: 14. Unified model of sedimentation, centrifugation and filtration of flocculated suspensions. *Int. J. Mineral Process.* **72**, 57–74.

[22] HAMPTON, R. E. (1997) Migration of particles undergoing pressure-driven flow in a circular conduit. *J. Rheol.* **41**(3), 621–640.

[23] HERMES, M., GUY, B. M., POON, W. C. K., POY, G., CATES, M. E. & WYART, M. (2016) Unsteady flow and particle migration in dense, non-Brownian suspensions. *J. Rheol.* **60**(5), 905–916.

[24] HORMOZI, S. & FRIGAARD, I. A. (2017) Dispersion of solids in fracturing flows of yield stress fluids. *J. Fluid Mech.* **830**, 93–137.

[25] ISA, L., BESSELING, R. & POON, W. C. K. (2007) Shear zones and wall slip in the capillary flow of concentrated colloidal suspensions. *Phys. Rev. Lett.* **98**, 198305.

[26] ISHII, M. & HIBIKI, T. (2011) *Thermo-Fluid Dynamics of Two-Phase Flow*, Springer, New York.

[27] JAMES, N., HAN, E., JURELLER, J. & JAEGER, H. (2017) Interparticle hydrogen bonding can elicit shear jamming in dense suspensions. arXiv:1707.09401v1 [cond-mat].

[28] JENKINS, J. T. & MCTIGUE, D. F. (1990) Transport processes in concentrated suspensions: The role of particle fluctuations. In: D. D. Joseph and D. G. Schaeffer (editors), *Two Phase Flows and Waves*, The IMA Volumes in Mathematics and Its Applications, Vol. 26, Springer, New York, pp. 70–79.

[29] KEYFITZ, B. L., SANDERS, R. & SEVER, M. (2003) Lack of hyperbolicity in the two-fluid model for two-phase incompressible flow. *Discrete Continuous Dyn. Syst. – Series B* **3**(4), 541–563.

[30] KOLEV, N. I. (2005) *Multiphase Flow Dynamics 1: Fundamentals*, Multiphase Flow Dynamics, Springer-Verlag, Berlin Heidelberg.

[31] Leighton, D. & Acrivos, A. (1987) Shear-induced migration of particles in concentrated suspensions. *J. Fluid Mech.* **181**(1), 415–439.

[32] D. Lhuillier, Chang, C.-H. & Theofanous, T. G. (2013) On the quest for a hyperbolic effective-field model of disperse flows. *J. Fluid Mech.* **731**, 184–194.

[33] Miller, R. M. & Morris, J. F. (2006) Normal stress-driven migration and axial development in pressure-driven flow of concentrated suspensions. *J. Non-Newton. Fluid Mech.* **135**(2–3), 149–165.

[34] Miller, R. M., Singh, J. P. & Morris, J. F. (2009) Suspension flow modeling for general geometries. *Chem. Eng. Sci.* **64**(22), 4597–4610.

[35] Morris, J. F. & Boulay, F. (1999) Curvilinear flows of noncolloidal suspensions: The role of normal stresses. *J. Rheol.* **43**, 1213–1237.

[36] Murisic, N., Pausader, B., D. Peschka & Bertozzi, A. L. (2013) Dynamics of particle settling and resuspension in viscous liquid films. *J. Fluid Mech.* **717**, 203–231.

[37] Nott, P. R. & Brady, J. F. (1994) Pressure-driven flow of suspensions: simulation and theory. *J. Fluid Mech.* **275**(1), 157–199.

[38] Oh, S., Song, Y.-Q., Garagash, D. I., Lecampion, B. & Desroches, J. (2015) Pressure-driven suspension flow near jamming. *Phys. Rev. Lett.* **114**(8).

[39] Phillips, R. J., Armstrong, R. C., Brown, R. A., Graham, A. L. & Abbott, J. R. (1992) A constitutive equation for concentrated suspensions that accounts for shear-induced particle migration. *Phys. Fluids A* **4**(1), 30–40.

[40] Prosperetti, A. & Jones, A. (1987) The linear stability of general two-phase flow models – II. *Int. J. Multiphase Flow* **13**(2), 161–171.

[41] Quemada, D. (1997) Rheological modelling of complex fluids. I. The concept of effective volume fraction revisited. *Eur. Phys. J. Appl. Phys.* **1**, 119–127.

[42] Quemada, D. (1998) Rheological modeling of complex fluids: III. Dilatant behavior of stabilized suspensions. *Eur. Phys. J. Appl. Phys.* **3**, 309–320.

[43] Quemada, D. (1998) Rheological modelling of complex fluids: II. Shear thickening behavior due to shear induced flocculation. *Eur. Phys. J. Appl.* **2**, 175–181.

[44] Quemada, D. (1999) Rheological modelling of complex fluids: IV: Thixotropic and "thixoelastic" behaviour. Start-up and stress relaxation, creep tests and hysteresis cycles. *Eur. Phys. J. Appl. Phys.* **5**(2), 191–207.

[45] Ramachandran, A. (2013) A macrotransport equation for the particle distribution in the flow of a concentrated, non-colloidal suspension through a circular tube. *J. Fluid Mech.* **734**, 219–252.

[46] Snook, B., Butler, J. E. & Guazzelli, É. (2016) Dynamics of shear-induced migration of spherical particles in oscillatory pipe flow. *J. Fluid Mech.* **786**, 128–153.

[47] Stickel, J. J. & Powell, R. L. (2005) Fluid mechanics and rheology of dense suspensions. *Annu. Rev. Fluid Mech.* **37**(1), 129–149.

[48] Trulsson, M., Andreotti, B. & Claudin, P. (2012) Transition from the viscous to inertial regime in dense suspensions. *Phys. Rev. Lett.* **109**(11), 118305.

[49] Whitaker, S. (1986) Flow in porous media I: A theoretical derivation of Darcy's law. *Trans. Porous Media* **1**(1), 3–25.

[50] Whitaker, S. (1998) *The Method of Volume Averaging*, Vol. 13, Springer, Netherlands, in: "Theory and Applications of Transport in Porous Media".

[51] Wyart, M. & Cates, M. E. (2014) Discontinuous shear thickening without inertia in dense non-brownian suspensions. *Phys. Rev. Lett.* **112**, 098302.

[52] Wylie, J. J., Koch, D. L. & Ladd, A. J. C. (2003) Rheology of suspensions with high particle inertia and moderate fluid inertia. *J. Fluid Mech.* **480**, 95–118.

[53] Yapici, K., Powell, R. L. & Phillips, R. J. (2009) Particle migration and suspension structure in steady and oscillatory plane Poiseuille flow. *Phys. Fluids* **21**(5), 053302.

[54] Zhou, J., Dupuy, B., Bertozzi, A. & Hosoi, A. (2005) Theory for shock dynamics in particle-laden thin films. *Phys. Rev. Lett.* **94**(11), 117803.

Appendix A Derivation of the two-phase flow model

A.1 Averaging rules

We will follow the mathematical framework by Drew and Passman [14,16] in this section. Let f and g be arbitrary measurable functions, c a constant and $\langle \cdot \rangle$ an average operator obeying the so-called Reynolds' rules

$$\langle f + g \rangle = \langle f \rangle + \langle g \rangle, \tag{A 1}$$

$$\langle \langle f \rangle g \rangle = \langle f \rangle \langle g \rangle, \tag{A 2}$$

$$\langle c \rangle = c, \tag{A 3}$$

the Leibniz' rule

$$\langle \partial_t f \rangle = \partial_t \langle f \rangle, \tag{A 4}$$

and the Gauss' rule

$$\langle \partial_i f \rangle = \partial_i \langle f \rangle. \tag{A 5}$$

The functions should be weakly differentiable up to the required order. Admissible operators are, for example, the volume average [30,49], time averages [26], the ensemble average [16] or a mixture of these [17]. However, note the derivatives are defined in the sense of distributions in this work. This implies $\langle \nabla f \rangle$ can have a Dirac delta property yielding additional surface integrals, whereas in classical theories the Leibniz' and Gauss' rule are written explicitly with surface integrals, cf. [16] and [49].

We further need a component indicator function

$$X_k(\boldsymbol{x}, t) = \begin{cases} 1, & \text{if } (\boldsymbol{x}, t) \in K \\ 0, & \text{if } (\boldsymbol{x}, t) \notin K, \end{cases} \tag{A 6}$$

with K the set of states of the kth-phase. In our model, we use the average operator in a weighted form. There are in general two averages in use, the intrinsic or phasic average

$$\overline{g} \equiv \frac{\langle X_k g \rangle}{\langle X_k \rangle}, \tag{A 7}$$

and the mass-weighted or Favré average (in its three common forms)

$$\widehat{g} \equiv \frac{\overline{\rho g}}{\overline{\rho}} = \frac{\langle X_k \rho g \rangle}{\langle X_k \rangle \frac{\langle X_k \rho \rangle}{\langle X_k \rangle}} = \frac{\langle X_k \rho g \rangle}{\langle X_k \rho \rangle}. \tag{A 8}$$

When we have multiple indicator functions, an index states the indicator function, we used in the average, e.g., $\overline{g}_s$ means we used X_s in the average. We define a fluctuation field (cf. [16]) as

$$g' := g - \overline{g}, \tag{A 9}$$

$$g^{\circ} := g - \widehat{g}, \tag{A 10}$$

and due to the Reynolds rules $\overline{g'} = \widehat{g^{\circ}} = 0$ holds. This splitting together with the Reynolds

rules yields the identity

$$\overline{fg} = \overline{f}\,\overline{g} + \overline{f'g'}, \tag{A 11}$$

and similar for the Favré average

$$\widehat{fg} = \widehat{f}\widehat{g} + \widehat{f^\circ g^\circ}. \tag{A 12}$$

The characteristic function fulfills the so-called topological equation (cf. [16])

$$\partial_t X_k + \boldsymbol{u}_i \cdot \nabla X_k = 0, \tag{A 13}$$

with $\boldsymbol{u}_i$ the interface velocity.

A.2 The two-phase flow model

Multiplication of (2.1a)–(2.1d) with X_k, followed by usage of the average operator and its linearity together with Gauss' and Leibniz' rules yield

$$\partial_t \langle X_k \rho \rangle + \nabla \cdot \langle X_k \rho \boldsymbol{u} \rangle = \langle \rho(\partial_t X_k + \boldsymbol{u}_i \nabla \cdot X_k) \rangle \tag{A 14}$$

$$+ \langle \rho(\boldsymbol{u} - \boldsymbol{u}_i) \cdot \nabla X_k \rangle, \tag{A 15}$$

$$\partial_t \langle X_k \rho \boldsymbol{u} \rangle + \nabla \cdot \langle X_k \rho \boldsymbol{u} \otimes \boldsymbol{u} \rangle - \nabla \cdot \langle X_k \boldsymbol{T} \rangle = \langle X_k \boldsymbol{f} \rangle \tag{A 16}$$

$$+ \langle (\partial_t X_k + \boldsymbol{u}_i \cdot \nabla X_k) \rho \boldsymbol{u} \rangle \tag{A 17}$$

$$+ \langle [(\boldsymbol{u} - \boldsymbol{u}_i) \cdot \nabla X_k] \rho \boldsymbol{u} \rangle - \langle \nabla X_k \cdot \boldsymbol{T} \rangle. \tag{A 18}$$

In the above, we assume that the interface velocity $\boldsymbol{u}_i$ has been smoothly extended for all x. Since the indicator function satisfies the so-called topological equation (cf. [16])

$$\partial_t X_k + \boldsymbol{u}_i \cdot \nabla X_k = 0, \tag{A 19}$$

the first- and the second-term equations (A 14) and (A 17) drop out, respectively, and we can write the system as

$$\partial_t \langle X_k \rho \rangle + \nabla \cdot \langle X_k \rho \boldsymbol{u} \rangle = \boldsymbol{\Gamma}_k, \tag{A 20}$$

$$\partial_t \langle X_k \rho \boldsymbol{u} \rangle + \nabla \cdot \langle X_k \rho \boldsymbol{u} \otimes \boldsymbol{u} \rangle \tag{A 21}$$

$$- \nabla \cdot \langle X_k \boldsymbol{T} \rangle = \langle X_k \boldsymbol{f} \rangle + \boldsymbol{M}_k, \tag{A 22}$$

where

$$\boldsymbol{\Gamma}_k \equiv \langle \rho(\boldsymbol{u} - \boldsymbol{u}_i) \cdot \nabla X_k \rangle, \tag{A 23}$$

$$\boldsymbol{M}_k \equiv \langle \nabla X_k \cdot [\rho(\boldsymbol{u} - \boldsymbol{u}_i) \otimes \boldsymbol{u} - \boldsymbol{T}] \rangle, \tag{A 24}$$

denotes the average interfacial mass source and the average interfacial momentum source for the kth phase, respectively.

To obtain the averaged form of the jump conditions, we note first the Dirac delta property of the component indicator functions' derivative

$$\langle \nabla X_k f \rangle = - \int_{\mathcal{S}_k} \boldsymbol{n}_k f_k \, d\boldsymbol{S}, \tag{A 25}$$

with $\mathcal{S}_k$ the interface of phase k. Using this and (A 23), (A 24) in the jump conditions for mass (2.1c) and momentum (2.1d), these conditions become

$$\sum_k \boldsymbol{\Gamma}_k = 0, \tag{A 26}$$

$$\sum_k \boldsymbol{M}_k = \boldsymbol{0}. \tag{A 27}$$

We further introduce the following averaged quantities

$$\phi_k \equiv \langle X_k \rangle,$$

for the volume fraction, and

$$\overline{\rho}_k \equiv \frac{\langle X_k \rho \rangle}{\phi_k},$$

$$\widehat{\boldsymbol{u}}_k \equiv \frac{\langle X_k \rho \boldsymbol{u} \rangle}{\phi_k \overline{\rho}_k},$$

$$\overline{\boldsymbol{T}}_k \equiv - \frac{\langle X_k \boldsymbol{T} \rangle}{\phi_k},$$

$$\boldsymbol{T}_k^{Re} \equiv - \frac{\langle X_k \rho \boldsymbol{u}_k^{\circ} \otimes \boldsymbol{u}_k^{\circ} \rangle}{\phi_k},$$

$$\overline{\boldsymbol{f}}_k \equiv \frac{\langle X_k \boldsymbol{f} \rangle}{\phi_k},$$

$$\boldsymbol{S}_k^d \equiv - \langle \nabla X_k \cdot \boldsymbol{T} \rangle,$$

$$\overline{\boldsymbol{u}}_{ki} \boldsymbol{\Gamma}_k \equiv \langle \nabla X_k \cdot \rho (\boldsymbol{u} - \boldsymbol{u}_i) \otimes \boldsymbol{u} \rangle,$$

for the average density, velocity, stress, Reynolds stress, body forces, interfacial stress and interfacial velocity of the kth phase, respectively.

Then, after we split the interfacial momentum source as

$$\boldsymbol{M}_k = \boldsymbol{S}_k^d + \overline{\boldsymbol{u}}_{ki} \boldsymbol{\Gamma}_k, \tag{A 28}$$

and the momentum flux into an average flux and a Reynolds stress

$$\langle X_k \rho \boldsymbol{u} \otimes \boldsymbol{u} \rangle = \phi_k \overline{\rho}_k \widehat{\boldsymbol{u}}_k \otimes \widehat{\boldsymbol{u}}_k - \phi_k \boldsymbol{T}_k^{Re}, \tag{A 29}$$

and use the product rule (A 12) for the velocity, we obtain the following system of phase

averaged mass and momentum equations

$$\partial_t(\phi_k\overline{\rho}_k) + \nabla \cdot (\phi_k\overline{\rho}_k\widehat{\boldsymbol{u}}_k) = \boldsymbol{\Gamma}_k, \tag{A 30}$$

$$\partial_t(\phi_k\overline{\rho}_k\widehat{\boldsymbol{u}}_k) + \nabla \cdot (\phi_k\overline{\rho}_k\widehat{\boldsymbol{u}}_k \otimes \widehat{\boldsymbol{u}}_k) - \nabla \cdot (\phi_k\overline{\boldsymbol{T}}_k) = \tag{A 31}$$

$$\nabla \cdot (\phi_k\boldsymbol{T}_k^{Re}) + \overline{\boldsymbol{f}}_k + \boldsymbol{S}_k^d + \overline{\boldsymbol{u}}_{ki}\boldsymbol{\Gamma}_k. \tag{A 32}$$

The Reynolds stress $\boldsymbol{T}_k^{Re}$ consists of two parts – liquid turbulence and pseudo-turbulence. As we are interested in the laminar flow regime, we neglect the liquid turbulence. Additionally, our derivations show $\boldsymbol{u}_f - \boldsymbol{u}_s$ has a very small value in the considered flow cases. Since the pseudo-turbulence scales as $(\boldsymbol{u}_f - \boldsymbol{u}_s)^2\phi_s$, see, e.g., [8,19], it will also be neglected. Further, we assume no phase change occurs at the interface between particles and liquid, $\boldsymbol{\Gamma}_k = 0$.

We introduce the stress tensor as the sum of pressure and deviatoric stress in the form

$$\boldsymbol{T} = -p\boldsymbol{I} + \boldsymbol{\tau}, \tag{A 33}$$

so that for the averaged quantities $\overline{\boldsymbol{T}}_k$ and

$$\overline{p}_k \equiv \frac{\langle X_k p \rangle}{\phi_k}, \tag{A 34}$$

$$\overline{\boldsymbol{\tau}}_k \equiv -\frac{\langle X_k \boldsymbol{\tau} \rangle}{\phi_k}, \tag{A 35}$$

we have correspondingly

$$\overline{\boldsymbol{T}}_k = -\overline{p}_k\boldsymbol{I} + \overline{\boldsymbol{\tau}}_k. \tag{A 36}$$

The interfacial pressure of phase k and the interfacial force density is defined as

$$\tilde{p}_{ik} \equiv \frac{\langle \nabla X_k p_k \rangle}{\langle \nabla X_k \rangle} = \frac{\langle \nabla X_k p_k \rangle}{\nabla \phi_k}, \tag{A 37}$$

$$\boldsymbol{M}_k^d \equiv \boldsymbol{S}_k^d - \langle \nabla X_k p_k \rangle = \langle \nabla X_k \cdot ((p_k - \tilde{p}_{ik})\boldsymbol{I} - \boldsymbol{\tau}) \rangle, \tag{A 38}$$

respectively, where the second equality in (A 37) follows from an application of Gauss' rule (A 5). We have (from (A 28))

$$\boldsymbol{M}_k = \boldsymbol{M}_k^d + \tilde{p}_{ik}\nabla \phi_k, \tag{A 39}$$

so that we obtain for the mass and momentum balance equations

$$\partial_t(\phi_k\overline{\rho}_k) + \nabla \cdot (\phi_k\overline{\rho}_k\widehat{\boldsymbol{u}}_k) = 0, \tag{A 40}$$

$$\partial_t(\phi_k\overline{\rho}_k\widehat{\boldsymbol{u}}_k) + \nabla \cdot (\phi_k\overline{\rho}_k\widehat{\boldsymbol{u}}_k \otimes \widehat{\boldsymbol{u}}_k) \tag{A 41}$$

$$-\nabla \cdot (\phi_k\overline{\boldsymbol{\tau}}_k) + \nabla(\phi_k\overline{p}_k) = \boldsymbol{M}_k^d + \tilde{p}_{ik}\nabla \phi_k, \tag{A 42}$$

where we have also assumed that no external body forces are applied, i.e., $\overline{\boldsymbol{f}} = 0$.

We neglect surface tension forces between the solid and the liquid phase, so the interfacial pressure difference becomes [14]

$$\sum_k \tilde{p}_{ik} \nabla \phi_k = 0, \tag{A 43}$$

and we obtain together with the interfacial momentum jump condition (A 27) the relation

$$M_s^d = -M_f^d. \tag{A 44}$$

Since we only have two phases, we know $\phi_s + \phi_f = 1$, which directly leads to $\nabla \phi_s = -\nabla \phi_f$. Thus, equation (A 43) yields

$$\tilde{p}_{is} = \tilde{p}_{if}.$$

For the case of identical liquid interfacial and bulk pressure

$$\tilde{p}_{if} = \overline{p}_f,$$

and constant densities $\overline{\rho}_k$ within each phase, the balance equations then reduce to the system (2.4).

Appendix B Boundary layer analysis for the drift-flux model

In this appendix, we complete the perturbation analysis used for the derivation of the drift-flux model in Section 4.1 by considering the inner layer near the wall. The purpose of this is to show that we recover the no-flux condition $w_2 = 0$ used to complete the drift-flux model (4.11), but we note that for a correct description of the density profile in the inner layer, which has a width $\varepsilon^{1/2} = \mathrm{Da}^{-1/2} \sim K_p^{1/2} \sim a$ i.e., of the size of the particles, we would have to include the possibility of a depletion layer, which, however, should not affect the no-flux condition on (4.11).

For the boundary layer analysis at the wall we introduce variable

$$z = \frac{\frac{1}{2} - y}{\varepsilon^{1/2}}, \qquad \Phi(t, z) = \phi(t, y). \tag{B 1}$$

Then, we obtain

$$\varepsilon^{1/2} \partial_t \Phi + \partial_z (\Phi (1 - \Phi) w_2) = 0, \tag{B 2a}$$

$$-\partial_z \left[(1 - \Phi) \partial_z v_1 + \varepsilon (1 - \Phi) \partial_z (\Phi w_1) \right] + \varepsilon (1 - \Phi) \partial_x p_f = -\varepsilon \frac{\Phi^2}{1 - \Phi} w_1, \tag{B 2b}$$

$$\varepsilon^{1/2} \partial_z \left[2 (1 - \Phi) \partial_z (\Phi w_2) \right] + (1 - \Phi) \partial_z p_f = \varepsilon^{1/2} \frac{\Phi^2}{1 - \Phi} w_2, \tag{B 2c}$$

$$-\partial_z \left[\Phi \eta_s \partial_z v_1 - \varepsilon \Phi \eta_s \partial_z ((1 - \Phi) w_1) \right] + \varepsilon \Phi \partial_x p_f = \varepsilon \frac{\Phi^2}{1 - \Phi} w_1, \tag{B 2d}$$

$$\varepsilon^{1/2} \partial_z \left[2 \Phi \partial_z ((1 - \Phi) w_2) \right] - \Phi \partial_z p_f - \partial_z p_c = \varepsilon^{1/2} \frac{\Phi^2}{1 - \Phi} w_2, \tag{B 2e}$$

and

$$p_c = \eta_n \left[\frac{1}{\varepsilon}(\partial_z v_1 - \varepsilon \partial_z((1 - \Phi)w_1))^2 + 2[\partial_z((1 - \Phi)w_2)]^2 \right]^{1/2}, \tag{B 2f}$$

and no-slip conditions at $z = 0$,

$$v_1 = 0, \quad w_1 = 0, \quad w_2 = 0. \tag{B 2g}$$

The leading order system is

$$\partial_z(\Phi(1 - \Phi)w_2) = 0, \tag{B 3a}$$

$$-\partial_z\left[(1 - \Phi)\partial_z v_1\right] = 0, \tag{B 3b}$$

$$(1 - \Phi)\partial_z p_f = 0, \tag{B 3c}$$

$$-\partial_z\left[\Phi \eta_s \partial_z v_1\right] = 0, \tag{B 3d}$$

$$-\partial_z p_c = 0, \tag{B 3e}$$

and

$$p_c = \eta_n \left[(\partial_z v_1)^2\right]^{1/2}, \tag{B 3f}$$

and no-slip conditions at $z = 0$,

$$v_1 = 0, \quad w_1 = 0, \quad w_2 = 0. \tag{B 3g}$$

We see immediately that $w_2 = 0$, which provides, via matching, the boundary condition for the drift-flux model at $y = 1/2$ as claimed in the text.